Decadal and long-term sea level variability in the tropical Indo-Pacific Ocean

**A. G. Nidheesh · Matthieu Lengaigne ·
Jérôme Vialard · A. S. Unnikrishnan ·
H. Dayan**

Abstract In this study, we analysed decadal and long-term steric sea level variations over 1966–2007 period in the Indo-Pacific sector, using an ocean general circulation model forced by reanalysis winds. The simulated steric sea level compares favourably with sea level from satellite altimetry and tide gauges at interannual and decadal timescales. The amplitude of decadal sea level variability (up to ∼5 cm standard deviation) is typically nearly half of the interannual variations (up to ∼10 cm) and two to three times larger than long-term sea level variations (up to 2 cm). Zonal wind stress varies at decadal timescales in the western Pacific and in the southern Indian Ocean, with coherent signals in ERA-40 (from which the model forcing is derived), NCEP, twentieth century and WASWind products. Contrary to the variability at interannual time-scale, for which there is a tendency of El Niño and Indian Ocean Dipole events to co-occur, decadal wind stress variations are relatively independent in the two basins. In the Pacific, those wind stress variations drive Ekman pumping on either side of the equator, and induce low frequency sea level variations in the western Pacific through planetary wave propagation. The equatorial signal from the western Pacific travels southward to the west Australian coast through equatorial and coastal wave guides. In the Indian Ocean, decadal zonal wind stress variations induce sea level fluctuations in the eastern equatorial Indian Ocean and the Bay of Bengal, through equatorial and coastal wave-guides. Wind stress curl in the southern Indian Ocean drives decadal variability in the south-western Indian Ocean through planetary waves. Decadal sea level variations in the south–western Indian Ocean, in the eastern equatorial Indian Ocean and in the Bay of Bengal are weakly correlated to variability in the Pacific Ocean. Even though the wind variability is coherent among various wind products at decadal timescales, they show a large contrast in long-term wind stress changes, suggesting that long-term sea level changes from forced ocean models need to be interpreted with caution.

Keywords Sea level · Steric level · Decadal variability · Climate

1 Introduction

The need to adapt to our time-evolving climate has raised great concern amongst scientists and policy makers due to the significant socio-economic and environmental consequences of these changes. Long-term (interannual to multi-decadal) climate variations are driven by a combination of anthropogenically forced climate change and natural climate variability. A clear understanding of the natural sea level variability at those timescales is crucial to confidently attribute the long-term sea level changes found in observations (see Cazenave and Nerem 2004; Bindoff et al. 2007). Even though the low-frequency sea level variations and the long term sea level trends along the Indian coast (Shankar and Shetye 1999; Unnikrishnan and Shankar 2007) as well as in the basin scale (Lee and McPhaden 2008; Cheng et al. 2008; Han et al. 2010) have been previously investigated, the picture of decadal/multi-decadal variability in the tropical Indo-Pacific region is still far from precise.

A. G. Nidheesh (✉) · M. Lengaigne · A. S. Unnikrishnan
Physical Oceanography Division, National Institute
of Oceanography, CSIR, Dona Paula, Goa 403004, India
e-mail: nidheeshag@gmail.com

M. Lengaigne · J. Vialard · H. Dayan
LOCEAN, IRD/CNRS/UPMC/MNHN, Paris, France

Natural and human-induced sea level trends in the Indo-Pacific region are embedded within a variety of timescales, ranging from intra-seasonal to multi-decadal. Amongst these different timescales, the most energetic is by far the seasonal one. This is particularly true in the Indian Ocean where the alternating northeast/southwest monsoon acts as a strong annual and semi-annual forcing that drives a basin-scale sea level response involving equatorial and coastal wave dynamics along the rim of the northern Indian Ocean (McCreary et al. 1993, 1996). At intra-seasonal timescales, the Indo-Pacific warm pool region is home to the Madden-Julian Oscillation, an eastward moving energetic fluctuation of deep atmospheric convection and surface winds in the 30–110 day range (Zhang 2005). These intra-seasonal wind signals drive surface current and sea level in the equatorial Indo-Pacific wave guide (Han 2005; Sengupta et al. 2007; Cravatte et al. 2003; Zhang et al. 2009) as well as along the northern coast of the Indian Ocean (Durand et al. 2009; Vialard et al. 2009; Oliver and Thompson 2010).

A large body of literature investigated the mechanisms responsible for interannual sea level variations in the Indo-Pacific region. Apart from the great whirl region off the east coast of Africa, where the variability is largely driven by the chaotic nature of ocean dynamics (Wirth et al. 2002), two climatic modes dominate the interannual sea level variations in the Indo-Pacific region: the El Niño Southern Oscillation (ENSO; McPhaden et al. 2006) and the Indian Ocean Dipole (IOD; Saji et al. 1999; Webster et al. 1999). Figure 1a illustrates the satellite observed mean sea level during October 1997–March 1998, a period characterized by the peak of a large El Niño in the Pacific (McPhaden et al. 1999) and a strong Indian Ocean Dipole in the Indian Ocean. During an El Niño, westerly wind anomalies in the central Pacific force eastward propagating Kelvin waves that depress the thermocline in the eastern Pacific cold tongue region (Fig. 1a). Those wind anomalies also force westward propagating Rossby waves that lift the thermocline in the western Pacific (Fig. 1a). A large number of observational and modelling studies (Clarke 1991; Clarke and Liu 1993; Meyers 1996; Masumoto and Meyers 1998; Potemra 2001, 2002; Wijffels and Meyers 2004; Cai et al. 2005a, b; Feng et al. 2003, 2005) showed that these Rossby waves initiate coastally trapped waves at the coast of Papua-New Guinea, which eventually propagate southward to the north Australian and west Australian coasts (the negative signals at the northern and western Australian coasts in Fig. 1a). Most of the sea level anomalies in the Indian Ocean are however linked to the dynamics of the Indian Ocean Dipole in the fall of 1997 (Fig. 1a). IOD-related easterly wind anomalies in the central Indian Ocean indeed force eastward propagating Kelvin waves, driving sea level interannual variations along the coast of Sumatra and the Bay of Bengal (Fig. 1a; Clarke and Liu 1994; Llovel et al.

2010; Rao et al. 2010). Finally, both IOD and ENSO induce Ekman pumping south of the equator in the Central Indian Ocean. This pumping forces Rossby waves that induce thermocline variations in the Seychelles-Chagos thermocline dome region (Masumoto and Meyers 1998; Tozuka et al. 2010). IOD events, however, rather drive sea level variations north of 10°S, while those south of 10°S are mainly forced by ENSO related wind forcing (Rao and Behera 2005; Yu et al. 2005).

Based on satellite observations of sea level and wind over the 1993–2006 period, Lee and McPhaden (2008) (hereafter LM08) revealed a near coherent large-scale decadal variability in much of the Indo-Pacific sector with a phase change at the end of the twentieth century (i.e. opposite trends during the 1993–2000 and 2000–2006 periods). Trade winds and sea level variations in the tropical Pacific and in the south Indian Ocean are anti-correlated during this period, implying anti-correlated variation of the sub-tropical cells in the two oceans. Figure 1b is identical to LM08 sea level trend estimate over the 2000–2006 period, and hence provides an estimate of typical decadal sea level change signals. At decadal timescales, regions of enhanced variability match relatively well with the regions at interannual timescales, although the amplitude of the signals are about half (Fig. 1b). Multi-decadal variations of sea level and sub-tropical cells have also been observed, although with a considerably weaker magnitude than their decadal counterpart (Zhang and McPhaden 2006; McPhaden and Zhang 2002, 2004). Similar to the variability at interannual timescales, decadal and multi-decadal sea level variations along the west Australian coast are coherent with those in the western Pacific, through oceanic tele-connections along equatorial and coastal wave guides (Feng et al. 2004, 2010). Tropical Pacific decadal and multi-decadal variability hence bears strong resemblance to interannual ENSO variations, leading Vimont (2005) to speculate that the oceanic processes at these timescales may be related to each other.

How much decadal and multi-decadal fluctuations may affect the detection of regional sea level changes due to anthropogenic climate change remains a debate (Cai et al. 2008; Zhang and Church 2011). Decadal sea level variability is indeed larger than available estimates of long-term trends (compare the estimates in Fig. 1b, c), and can hence strongly alias estimates of long-term trends. For example, estimates of trends since the early 1990's, indicate sea level increase in the western tropical Pacific (Feng et al. 2010; Carton et al. 2005). This supports the notion of a strengthening Hadley circulation in recent decades (Mitas and Clement 2005) and appears to partly contradict observational and modelling results highlighting a weakening of the tropical circulation in the Pacific in response to global warming at longer time-scales (Vecchi et al. 2006; Vecchi and Soden 2007; Yu and
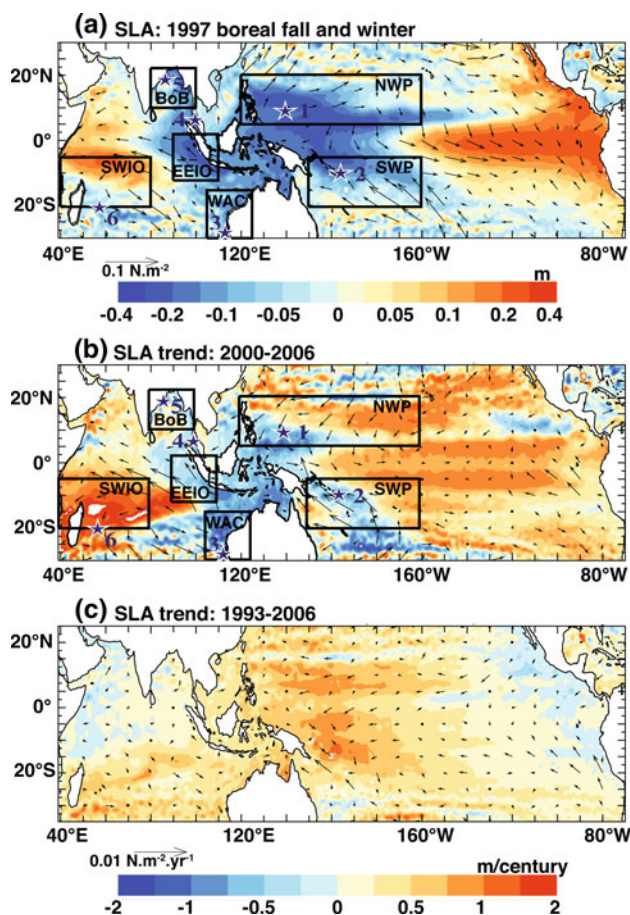
Fig. 1 **a** Satellite SLA during October 1997-March 1998 (*color*) and associated wind anomaly derived from NCEP (*arrow*). **b** Satellite SLA linear trend for the 2000–2006 period (*color*) and associated NCEP wind stress trend (*arrow*). **c** Satellite SLA linear trend for the 1993–2006 period (*color*) and associated NCEP wind stress trend (*arrow*). The mean seasonal cycles were removed from both SLA and wind datasets. The *stars* on **a** and **b** indicate locations of the tide-gauges used to validate the model steric sea level. The selected gauge locations are (1) Yap B (138°E, 9.5°N), (2) Honiara II (161°E, 9.5°S), (3) Fremantle (115.7°E, 32°S), (4) Langkawi (99.8°E, 6.4°N), (5) Paradip (86.7°E, 20.3°N) and (6) Port Louis (57.5°E, 20.15°S). *Boxes* on (**a**) and (**b**) indicate the regions where model will be validated to satellite observations. The selected *boxes* are the North West Pacific (NWP), the Western Australian Coast (WAC), the South West Pacific (SWP), the Eastern Equatorial Indian Ocean (EEIO), the Bay of Bengal (BoB) and the South West Indian Ocean (SWIO). **b** Is identical to fig. 1c of Lee and McPhaden (2008), i.e. an estimate of decadal sea level variations over that period. Panel **c** provides an estimate of long-term sea level trends over 1993–2006, the period consistent with the study by Lee and McPhaden (2008). Units are in m for **a** and m/century for **b**, **c**

Zwiers 2010; Tokinaga et al. 2012). But trends estimated over a longer period (1958–2001) show a multi-decadal sea level decrease in the South Pacific (Timmermann et al. 2010), which can be linked to changes in the wind stress curl related to the weakening of trade winds in the Pacific (Vecchi et al. 2006). In the Indian Ocean, trends over the altimeter period (Fig. 1c) are strikingly different from estimates over

longer periods (1960–1999 in Alory et al. 2007, 1961–2008 for Han et al. 2010), which show that sea level has substantially decreased in the south tropical Indian Ocean while it has increased elsewhere. Han et al. (2010) attributed this basin-wide feature to changes in the surface winds partly attributable to rising levels of anthropogenic greenhouse gases. Alory et al. (2007) and Schwarzkopf and Böning (2011) suggested that the trend discussed by Timmermann et al. (2010) in the Pacific may also be transmitted to the Indian Ocean by the Indonesian throughflow and hence partly explain the observed sea level decrease in the south tropical Indian Ocean.

The above studies indicate that there is still a lot of discrepancy in the description of long-term changes in sea level variations and their causes. A better understanding of the dynamics of decadal to multi-decadal natural variability is therefore crucial for the attribution of observed long-term trends in the climate system (Meehl et al. 2009a, b). Only a few studies have so far investigated the decadal sea level variability in the Indian Ocean, either focusing on the recent satellite period (LM08) or on the western Pacific-west Australian coast oceanic connection using tide gauge data (Feng et al. 2010). In this paper, we aim at describing and understanding the decadal variability of the Indo-Pacific region over a 42 years period using an ocean general circulation model (OGCM) validated against available observations. Although our focus will be more on the Indian Ocean, we consider the entire Indo-Pacific region owing to the known Indo-Pacific connections (Feng et al. 2010) and also discuss interannual variability as a basis of comparison for decadal fluctuations. Section 2 describes the numerical simulations and the observed datasets used for validation, as well as the method used to extract the signals at different timescales. Section 3 validates the sea level variations in our OGCM simulation against satellite and tide gauge datasets. In Sect. 4, interannual and decadal sea level variations and the related atmospheric forcing and oceanic mechanisms are described for the entire Indo-Pacific region. We also assess the robustness of the decadal forcing of the model (largely based on the ERA-40 re-analysis) by comparing it with three other wind products. In Sect. 5, we briefly describe the long-term steric sea level (1966–2007) trends in our model, and the corresponding wind forcing trends in three other wind products. A summary with concluding remarks is provided in the final section.

2 Datasets and methods

2.1 Observational datasets

We used altimeter measurements of sea surface height (SSH) and in situ measurements of sea level from tide

gauges to validate the model steric sea level variations. The satellite SSH data combine the joint US-French missions TOPEX/POSEIDON (October 1992–October 2002) and JASON-1 or Envisat (October 2002–present). The data have been processed by CLS Space Oceanography Division and distributed over weekly intervals on a one-third degree Mercator grid. The weekly data were converted into monthly-averaged sea level data and those monthly data were used in the present study.

Since the sea level from altimetry covers only the last two decades, we also used historical tide gauge data obtained from the Permanent Service for Mean Sea Level (PSMSL—Woodworth and Player 2003). As many of the gauge stations in the Indo-Pacific region suffer from large data gaps, we selected a few tide gauge stations (with shortest gaps in regions of largest decadal variability). The selected gauge locations, shown as stars on Fig. 1a are 1. Yap B (138°E; 9.5°N), 2. Honiara II (161°E; 9.5°S), 3. Fremantle (115.7°E; 32°S), 4. Langkawi (99.8°E; 6.4°N), 5. Paradip (86.7°E; 20.3°N) and 6. Port Louis (57.5°E; 20.15°S). The representativeness of these local data with respect to the box-averaged regions will be discussed in Sect. 3.

2.2 Ocean model experiment

The numerical simulation used in this study is from the DRAKKAR project (Brodeau et al. 2010), and is based on NEMO (Nucleus for European Modelling of the Ocean, formerly known as OPA) Ocean General Circulation Model (hereafter, OGCM, Madec 2008). The model is based on the standard primitive equations, uses a free surface formulation (Roullet and Madec 2000) and computes the density from potential temperature, salinity and pressure using the Jackett and McDougall (1995) equation of state.

The experiment in this study uses an eddy permitting ¼° resolution. The vertical grid has 46 levels with a 6-m spacing at the surface increasing to 250-m in the deep ocean. Bathymetry is represented with partial steps (Barnier et al. 2006). Vertical mixing is computed from a turbulence closure scheme based on a prognostic vertical turbulent kinetic equation, which performs well in the tropics (Blanke and Delecluse 1993). Lateral mixing acts along isopycnal surfaces, with a Laplacian operator and a constant $200 \ m^2 \ s^{-1}$ isopycnal diffusivity coefficient (Lengaigne et al. 2003). Short-wave fluxes penetrate into the ocean based on a single exponential profile (Paulson and Simpson 1977) corresponding to oligotrophic water (attenuation depth of 23 m).

The model is forced with the 1958–2004 DFS3 dataset described in detail in Brodeau et al. (2010). This forcing is essentially based on the corrected ERA-40 re-analysis (Uppala et al. 2005, and ECMWF operational analyses beyond 2002) for near surface meteorological variables and on the

corrected ISCCP-FD radiation product (Zhang et al. 2004) after 1984. No surface temperature restoring is used and salinity is restored to climatological values, with a relaxation time scale of 33 days (for a 10 m thick layer). The model simulation is initialized in 1958 with Levitus et al. (1998) climatology. The model is then run over the 1958–2007 period, using the DFS3 forcing. Because this study aims at investigating interannual to decadal timescales, the beginning of this simulation has to be discarded (until the model has "forgotten" the initial shock at the beginning of 1958). We did discard the first 8 years of this simulation (1958–1965) and analysed the output only for the 1966–2007 period. This choice of discarding the first 8 years can be justified as follows: i) empirical orthogonal function (EOF) analysis of the steric sea level over the full period (1958–2007) shows a first EOF whose principal component changes steeply over the first 8 years and then remain quite flat; ii) the typical first-baroclinic mode planetary wave phase velocity is about $0.05 \ m \ s^{-1}$ at 30° latitude (i.e., 12,000 km in 8 years), and about $0.1 \ m \ s^{-1}$ at 20° latitude i.e. 24,000 km in 8 years (Chelton and Schlax 1996): this leaves enough time for basin-scale adjustment within the tropics.

The OGCM has been extensively validated with various forcing strategies in uncoupled mode (e.g. Vialard et al. 2001; Cravatte et al. 2007) and in coupled mode (e.g. Lengaigne et al. 2006; Lengaigne and Vecchi 2009). This model accurately simulates equatorial dynamics and basin wide structures of currents and temperature in the tropics. The particular simulation analysed in this paper also reproduces observed equatorial currents and interannual variations of the heat content in the tropical Pacific (Lengaigne et al. 2012) and mixed layer depth in the Indian Ocean (Keerthi et al. 2012) accurately.

2.3 Surface wind products

Estimates of long term variations from re-analyses (such as the ERA-40 reanalysis, on which the model forcing is based) are subject to spurious variations caused by changes in the observing system, or measurement methods (e.g. the effect of anemometer height discussed in Tokinaga and Xie 2011). To assess the robustness of the model wind forcing, we compared the decadal variability with other wind datasets covering the entire 1958–2007 period, namely the NCEP and twentieth century re-analyses and the WASWind dataset. The NCEP/NCAR reanalysis uses a state-of-the-art analysis/forecast system to perform data assimilation using past data from 1948 to the present, with an original ∼1.9° resolution (Kalnay et al. 1996). The twentieth century reanalysis project (Compo et al. 2010) is an effort to produce a reanalysis dataset spanning the entire twentieth century, assimilating surface pressure and sea level observations from the International Surface Pressure Databank station component

version 2 (Yin et al. 2008), International Comprehensive Ocean–Atmosphere Data Set (ICOADS, Woodruff et al. 2011) and from the International Best Track Archive for Climatic Stewardship (IBTrACS, Knapp et al. 2010) in every 6 h. This dataset offers 6-hourly wind data from 1870 to 2008. Finally, we also used a new surface wind dataset from the wind speed and wind wave-height ship observations archived in the ICOADS database. This Wave and Anemometer-based Sea surface Wind (WASWind; Tokinaga and Xie 2011) dataset is corrected for spurious upward trend due to increases in anemometer height and provides wind velocity and scalar speed at monthly resolution on a $4° \times 4°$ longitude–latitude grid from 1950 to 2008. All these datasets were interpolated onto the regular $2.5° \times 2.5°$ NCEP grid to ease comparison.

2.4 Methods

Changes in temperature and salinity in a water column result in changes in vertical height of the column, referred to as 'steric' sea level variations (Pattullo et al. 1955). Changes caused by temperature and salinity variations are respectively referred as the thermosteric and halosteric sea level anomalies (hereafter TSLA and HSLA). The sum of TSLA and HSLA is the total steric sea level anomaly (SSLA). SSLA variations have been computed for the upper thousand meter layer of the Indo-Pacific ocean from the model temperature and salinity fields as follows:

$$TSLA = \int_{z=0}^{1,000} \frac{1}{v} \frac{\partial v}{\partial T} \Delta T \, dz \quad HSLA = \int_{z=0}^{1,000} \frac{1}{v} \frac{\partial v}{\partial S} \Delta S \, dz$$

(see Antonov et al. 2002) in which v is specific volume, z is depth and ΔT and ΔS are the temperature and salinity anomalies computed by subtracting the mean temperature and salinity field for the entire period from the raw values at each standard depth. Specific volume v has been computed at each standard depth level as a function of monthly mean temperature and salinity fields and pressure using the 1980 equation of state for sea water (UNESCO 1981; Millero and Poisson 1981).

Because of the Boussinesq approximation, the model global average sea level does not account for a sea level rise due to a net thermal (or haline) expansion/contraction (Greatbatch 1994), i.e. the global average ocean *mass* can vary under the effect of a surface buoyancy flux imbalance, but not the global average *sea level*. We hence use steric sea level variations, rather than the sea level in the free-surface NEMO simulation in our analyses because: i) it can account for a basin-average sea level increase due to a uniform buoyancy flux and ii) it does not include the long-term sea level drift caused by unbalanced freshwater (evaporation minus precipitation and runoff) over the

global ocean in the forcing dataset. Since the changes in steric sea level are an important contribution to local changes in sea level on seasonal and climatic time scales (Pattullo et al. 1955; Church et al. 1991; Gregory 1993), it is reasonable to assume that the steric sea level variations discussed in this study are more or less equivalent to the actual sea level variations.

The interannual and decadal signals of the monthly SSLA data were extracted using the STL (Seasonal-Trend decomposition procedure based on Loess) filtering method (Cleveland et al. 1990). STL is a robust iterative non-parametric regression procedure using loess smoother, which allows decomposing a time series into long-term, seasonal and remainder components. As for all non-parametric regression methods, STL requires subjective selection of a smoothing parameter to define the lowest frequency component. We chose a 7-year threshold to extract long-term (decadal) component in the steric sea level data. Results from this procedure are illustrated on Fig. 2 for SSLA variations in the northwest Pacific. The STL method successfully extracts the seasonal variations (Fig. 2b) as well as the long-term evolution (Fig. 2d) accounting for SSLA variations with timescales larger than 7 years. The remainder (Fig. 2c) is the residual of the full field once the seasonal and long-term components subtracted and will be referred to as interannual sea level in the following sections. Sensitivity tests using cut-off period ranging from 4 to 8 years were performed for the extraction of long-term component and we found that the main results and conclusions of this study were not altered. This method was applied both to the steric field and to the various wind products described above to extract signals in decadal timescales.

In Sects. 3 and 4 of this paper, we will focus on decadal sea level and wind forcing variations (and interannual variations, for comparison purposes). We will briefly discuss multi-decadal variability in the model outputs and several forcing products in Sect. 5. We define *interannual* variations as the residual after applying the STL procedure (i.e. monthly anomalies with respect to the seasonal cycle, with time scales less than 7 years). We isolate *multi-decadal* variability, either linked to anthropogenic or natural climate variations, from the linear trends of the STL-derived long-term component over the 1966–2007 period (see Fig. 2d for an example). We obtain the *decadal* variability as the difference between the STL derived long-term component and this linear trend (Fig. 2d).

3 Observed and modelled variability in key regions

The ocean model experiment discussed in this paper reproduced interannual variability in the Pacific (Lengaigne et al. 2012) and Indian Oceans (Keerthi et al. 2012) accurately. It is
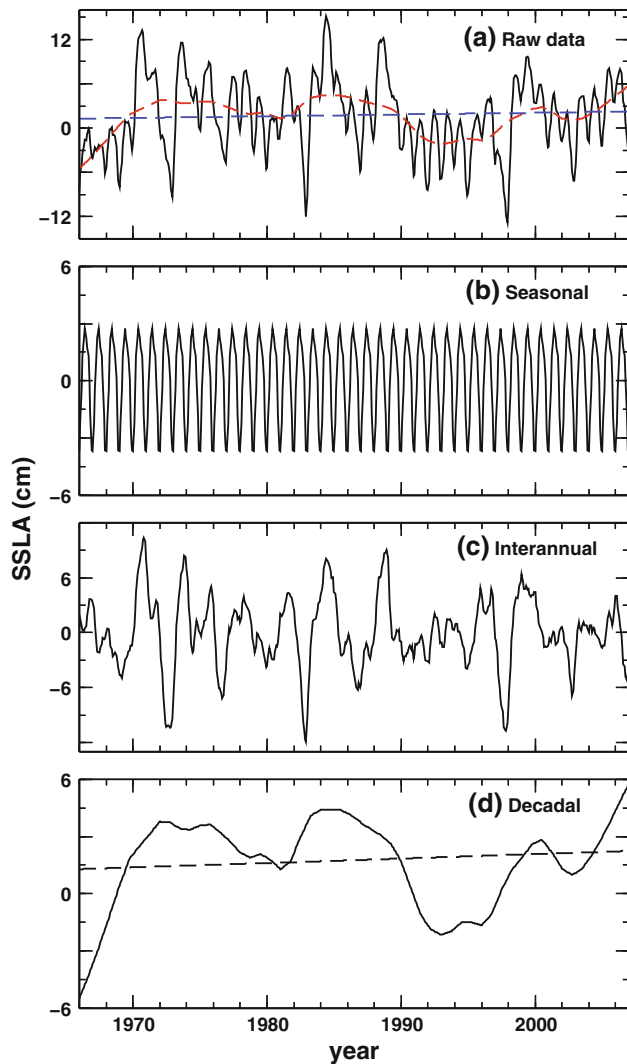
Fig. 2 Time series of model steric sea level variations in the Northwest Pacific, extracted by STL method: **a** raw data (*black curve*), **b** seasonal, **c** interannual and **d** decadal component. The linear trend associated with multi-decadal variability is shown as a *dashed line* in **d**. This linear trend has been subtracted from estimates of decadal variability discussed in this paper. The components shown in **d** are also shown in **a**

more difficult to validate decadal variability, for which suitable long records are rare. Figure 3 shows regions of strong interannual, decadal and multi-decadal SSLA variations. Figure 3 will be further discussed in Sect. 4, but is mentioned here in order to define regions of strong variations for which the model to be validated. We define six regions of relative maxima in decadal SSLA variations, which also display clear variations at interannual timescales: the Northwest Pacific (NWP—120°E:200°E, 5°N:20°N), West Australian Coast (WAC—105°E:125°E, 15°S:30°S), Southwest Pacific (SWP—150°E:200°E, 5°S:20°S), Eastern Equatorial Indian Ocean (EEIO—90°E:110°E, 2°N:12°S), Bay of Bengal (BoB—80°E:100°E, 10°N:22°N) and the

Southwest Indian Ocean (SWIO—40°E:80°E, 5°S:20°S). We also selected one tide-gauge time series record, within each of these regions. The representativeness of the location of tide gauges with respect to the large-scale region (shown by boxes in Fig. 1) is illustrated in Table 1, which displays the correlation between the box-averaged model steric sea level and the steric sea level at the corresponding tide gauge location, at interannual and decadal timescales. In the western Pacific (NWP, SWP), in the eastern equatorial Indian Ocean (EEIO) and along the west Australian coast (WAC), the selected tide gauges are very representative of the whole region at both interannual and decadal timescales (correlation ranging from 0.79 to 0.96). The Paradip tide gauge is less representative of the entire Bay of Bengal with correlations of ~ 0.65 at both timescales. Finally, the interannual sea level evolution at the tide gauge of Port Louis is not representative of the interannual evolution in the SWIO box ($r = 0.33$), while it is more representative at decadal timescales ($r = 0.56$).

The ability of the model to simulate the sea level evolution in the selected regions is illustrated in Fig. 4, which compares the evolution of the model SSLA anomalies (green curves) with regionally-averaged altimeter data (red curves, left panel) and selected tide gauge data (blue curves, right panel). Interannual and decadal variations from model outputs compare both remarkably well with satellite and tide gauge estimates in the NWP, SWP and WAC (correlations ranging from 0.71 to 0.95). The model SSLA evolution at decadal timescales in the NWP and WAC also agrees well with the Feng et al. (2010) observational analysis using tide gauge data (their Fig. 3). In the EEIO, the model compares well with the satellite estimates, with a correlation of above 0.85. Model and tide gauge data also display a very good agreement at Langkawi in the eastern Indian Ocean and a reasonably good match at Paradip station along the western Bay of Bengal. At Port Louis, on the southern border of the SWIO region, the IOD influence is rather weak (see Fig. 1a and Table 1), and the model does not capture interannual sea level variations properly. On the other hand, the decadal evolution is similar to the tide gauge data from the mid-80's onward.

Apart from an accurate model evolution over the periods where observations are available, Fig. 4 also reveals evident connections between sea level variability in several regions at both interannual and decadal timescales. The strength of the relationship between sea level evolution in various regions or at various tide gauge locations for both model and observations is provided in Table 2, while Table 3 allows to discuss the oceanic tele-connections inferred from the model SSLA at interannual and decadal timescales. Sea level variations in NWP and WAC display a very similar evolution (Fig. 4), with correlation between 0.6 and 0.8 at the tide gauge location and regionally, the
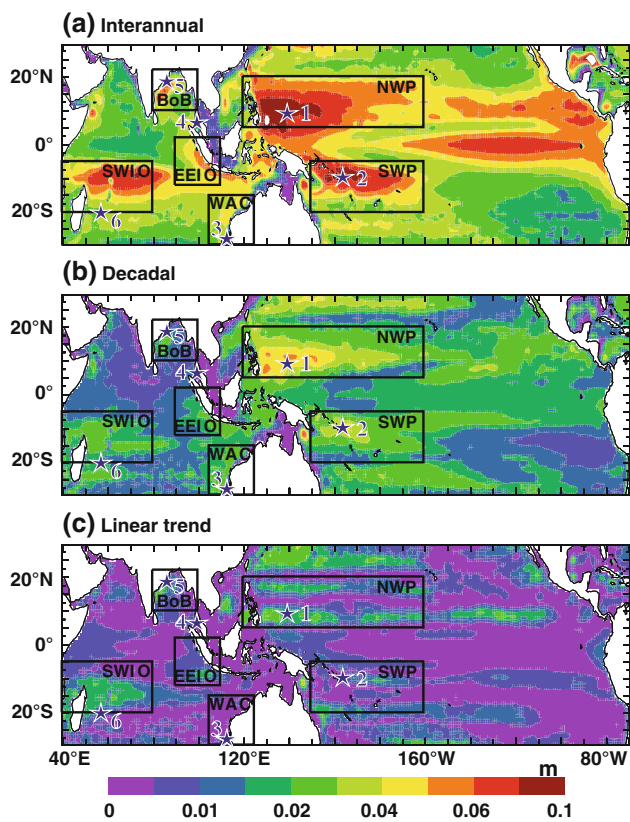
Fig. 3 Standard deviation of model steric sea level variations over the 1966–2007 period for (**a**) interannual timescales, (**b**) decadal timescales and (**c**) long-term linear trend. The *boxes* on each panel (similar to those on Fig. 1) indicate regions of strong interannual and decadal variability. The locations of tide gauge data used in this study are also indicated by *stars*

Table 1 Correlation coefficient between model SSLA evolution averaged over the box (see Figs. 1, 3) and at the corresponding tide gauge location at interannual and decadal timescales over the 1966–2007 period

Regions/tide gauge	Interannual	Decadal
NWP/Yap B	0.83	0.93
WAC/Fremantle	0.79	0.89
SWP/Honiara	0.86	0.85
EEIO/Langkawi	0.91	0.96
BOB/Paradip	0.68	0.63
SWIO/Port Louis	0.33	0.56

NWP signal leading the WAC signal by 0–4 months (Table 2). This strong relationship holds good for both interannual (r = 0.79) and decadal (r = 0.64) timescales. At interannual timescales, there are indeed relative minima during El Niño events (e.g. in 1972, 1982, 1987, 1997) and relative maxima during La Niña events (e.g. in 1975, 1984, 1988, 1999)[1] for both locations. The NWP and WAC regions also display a comparable decadal evolution (black curves), with a maximum in the mid-1970's, mid-1980's and around 2000 and a minimum in the 1960's, in the early 1980's, in the early 1990's and in the mid-2000's in both regions.

Regionally averaged sea level signals in SWP and NWP also display a good agreement between the model SSLA and satellite estimates, with a correlation around 0.6. The agreement is weaker at tide gauge locations, where correlation of about 0.5 for both datasets (Table 2) is found. As illustrated in Table 3, this co-variability between NWP and SWP holds true for both interannual and decadal variations.

At interannual timescales, both locations display relative minima during El Niño events and relative maxima during La Niña, the SWP lagging the NWP signal by 6 months (Tables 2, 3). This co-variability is even slightly stronger for decadal timescales (r = 0.71) compared to interannual timescales (r = 0.63).

The EEIO exhibits very clear signatures of IOD events at interannual timescales with negative SSLA anomalies during positive IOD events (e.g. in 1982, 1994, 1997, 2007) and positive SSLA anomalies during negative IOD events (e.g. in 1985, 1988/89, 1996). Most of these extrema are also present in the Bay of Bengal (BoB), which displays a very similar evolution to the EEIO, with correlations above 0.8 (with no lag) for both model and observations (Table 2). At decadal timescales, variations in the BoB agree well with variations in the EEIO (r = 0.85; Table 3) with an increase from the late 60's until the early 80's, a minimum in the mid-90's and a maximum in the early 2000's (Fig. 4g, i).

The steric sea level evolution averaged over the boxes shown in Fig. 1 indicates that variations in the SWIO region are significantly anti-correlated with those in the EEIO and NWP, with correlation below −0.7 (Table 2). The relationship between the variability in the SWIO and EEIO/NWP regions is evident at interannual timescales, with positive IOD events associated with positive sea level anomalies in SWIO and negative in EEIO (e.g. in 1994 and 1997). When considering tide gauge locations, this anti-correlation is considerably weaker, (correlation ∼ −0.35) for both model and observations. This mismatch between the results for box averages and tide gauge locations can be understood as follows: The IOD signal is rather weak at Port Louis station, which is located at the very southern border of the SWIO box (Fig. 1a; Table 1). Sea level signal at Port Louis is dominated to a large extent by decadal variations (in contrast to the box average): at this timescale, the SWIO stands out as partly independent from other regions (last two lines of Table 3): while SWIO and EEIO exhibit opposite decadal evolution during the last 10 years of the simulation, there is no obvious relationship during the early part of the simulation (Fig. 4g, k).
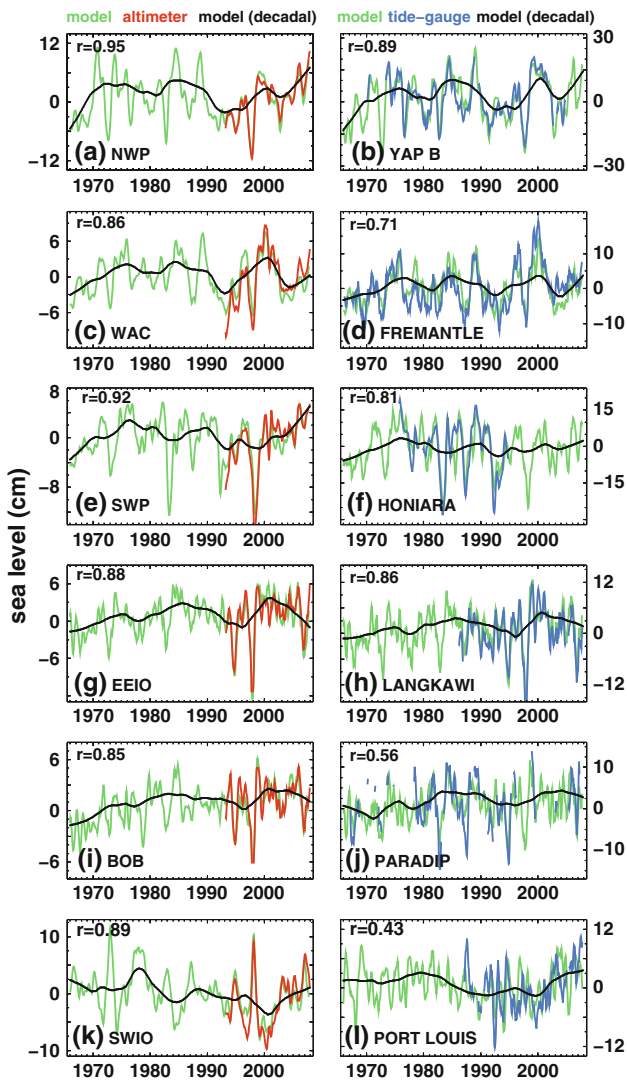
---

[1] ENSO and IOD years are taken from Ummenhoefer et al. (2009).

Fig. 4 Comparison of monthly model steric sea level anomalies with altimeter (*left panel*) and tide gauge sea level anomalies (*right panel*). Time series on the *left panels* are averaged over the regions shown on Figs. 1 and 3 while time series on the *right panels* are extracted at the corresponding tide gauge locations indicated by *stars* on Figs. 1 and 3. The monthly anomalies were calculated by removing the mean seasonal cycle and a 5 months smoothing is further applied to the time-series. The linear correlation coefficient between the model and observed time-series is given on the *top left* of each panel. The *black line* indicates the model decadal signal (including long-term linear trend)

Finally, the long-term linear trends computed from the simulated SSLA and observed sea level at tide gauge locations are given in Table 4. This Table first illustrates that for the six regions, the model displays a long-term trend of the same sign as the considered tide gauge, with a sea level rise at all stations in the Indian Ocean (Fremantle, Langkawi, Paradip and Port Louis) and a decrease in the western Pacific (Yap B and Honiara). While the model reasonably captures the amplitude of the observed

long-term trend at Honiara, Langkawi, Paradip and Port Louis, the model SSLA trend is larger than the tide gauge trend at Yap B and weaker at Fremantle. When the SSLA trend is calculated over the entire model period (values in bracket), its value varies considerably, even changing in sign at Yap B and becoming negligible at Port Louis and Honiara. This illustrates the strong sensitivity of the sea level trend to the considered period, which can partly be attributed to the aliasing by the interannual and decadal variability, further illustrated in Sect. 5.

To summarize, the above results demonstrate that the model captures interannual and decadal sea level variations reasonably well, over periods where observational estimates from satellite and tide gauge data are available. In addition, our analysis suggests that interannual and decadal variations in both model and observations are very similar between the WAC, NWP and SWP regions and between the EEIO and BoB while the SWIO region stands out as partly independent from other regions of the Indo-Pacific sector at decadal timescales. In the following, we therefore use the modelled SSLA with some confidence to infer the interannual and decadal sea level variability at the basin scale over the 1966–2007 period and investigate the main processes responsible for these changes.

4 Decadal sea level variations and related mechanisms

4.1 Overall description

Figure 3a, b shows the standard deviation of the model SSLA for both interannual and decadal timescales. Regions of maximum decadal variability are also home to strong interannual fluctuations in the western Pacific and the Indian Ocean (NWP, SWP, SWIO, EEIO, WAC and BOB). This may indicate some relationship between the variability at these two time scales, even though the amplitudes at decadal timescales are nearly half than those in interannual variations in NWP, SWP and WAC and half to one-third in EEIO, BoB and SWIO. It is to be noted, however, that while interannual variability displays a clear maximum in the eastern equatorial Pacific, explained by Kelvin wave response to interannual wind anomalies, no such maximum appears at decadal timescales. The coherent pattern of long-term variability diagnosed in the model for the SWIO (Fig. 3c) has been discussed by Han et al. (2010), who suggested that it is due to more intense Walker and Hadley circulation in the Indian Ocean, partly attributable to rising levels of atmospheric greenhouse gases. Figure 3, however, illustrates that this long-term trend has considerably weaker amplitude in most of the Indo-Pacific sector as compared to both interannual and decadal variations, ranging from a bit less than twice weaker than decadal

Table 2 Maximum lag-correlation of sea level anomalies between different regions in the Indo-Pacific sector for model and observations (either tide gauges or satellite)

Regions	Gauge location		Box average	
	Tide Gauge	Model	Satellite	Model
NWP/WAC	0.76^{+0}	0.71^{+2} (0.76^{+1})	0.79^{+3}	0.75^{+3} (0.74^{+4})
NWP/SWP	0.52^{+6}	0.36^{+8} (0.53^{+6})	0.62^{+7}	0.61^{+7} (0.58^{+8})
EEIO/BOB	0.79^{+0}	0.89^{+0} (0.81^{+0})	0.91^{+1}	0.86^{+2} (0.80^{+1})
EEIO/NWP	0.68^{+0}	0.62^{+0} (0.57^{-1})	0.68^{-1}	0.67^{-1} (0.61^{-2})
SWIO/EEIO	-0.33^{-3}	-0.35^{+2} (-0.19^{+1})	-0.78^{+3}	-0.91^{+3} (-0.72^{+2})
SWIO/NWP	-0.37^{-4}	-0.36^{-2} (-0.14^{-5})	-0.76^{-4}	-0.84^{-4} (-0.47^{-5})

The exponent indicates the lag of maximum correlation, in months. For the model, bold values indicate lag-correlations over the period when observations are available while values in parentheses indicate lag-correlations for the entire 1966–2007 period. Anomalies have been calculated by removing the mean seasonal cycle and the long-term linear trend. A 5 months smoothing is further applied to the resulting time series

Table 3 Correlation coefficient of model steric sea level evolution between selected regions in the Indo-Pacific sector at interannual and decadal time-scales

Regions	Interannual	Decadal
NWP/WAC	0.79^{+4}	0.64
NWP/SWP	0.63^{+8}	0.71
EEIO/BOB	0.79^{+1}	0.85
EEIO/NWP	0.65^{-1}	0.47
SWIO/EEIO	-0.84^{-2}	−0.42
SWIO/NWP	-0.69^{-5}	0.08

The various regions are shown on Figs. 1, 3 and 7

Table 4 Linear trend of observed sea level and model steric sea level at tide gauge locations

Tide gauge location	Tide-gauge (m/century)	Model (m/century)
Yap B	**−0.055**	**−0.126** (0.137)
Fremantle	**0.137**	**0.029** (0.034)
Honiara	**−0.482**	**−0.446** (−0.001)
Langkawi	**0.067**	**0.053** (0.077)
Paradip	**0.092**	**0.069** (0.089)
Port Louis	**0.203**	**0.311** (−0.006)

For the model, bold values indicate linear trends calculated over the period when observations are available while the values in parenthesis indicate the linear trend calculated over the entire 1966–2007 period

variations in the BoB and SWIO to more than three times weaker in the western Pacific.

As revealed by Fig. 5, decadal SSLA variations are almost entirely driven by thermosteric variations, with halosteric variations playing a significant role in only a few regions (e.g. western Indonesian seas and north of Australia), where amplitude of decadal signals are weak (Fig. 5b). A similar conclusion can be drawn for interannual timescales (not shown). Interannual and decadal variations discussed in the following sections are hence essentially associated with the temperature changes in the upper thousand meters layer over the Indo-Pacific ocean.

4.2 Basin-scale pattern of sea level variations

The large-scale interannual and decadal SSLA variations in the Indo-Pacific region were inferred using an empirical orthogonal function (EOF) analysis. The first two EOF modes as well as the corresponding principal components for both interannual and decadal timescales are displayed in Fig. 6. These two modes represents more than 60 % of the total variance at decadal timescales. The regression coefficients of the zonal and meridional wind stress to the normalized PC of each EOF have also been overlaid in each panel.

At interannual timescales, the first two modes respectively explain 41 and 16 % of the total variance, with each of the higher modes represent less than 5 %. These EOF modes for interannual timescales agree well with a similar analysis performed on the D20 of the BMRC reanalysis in the tropical Pacific by Meinen and McPhaden (2000) over the 1980–1999 period (their Fig. 3). The first mode (Fig. 6a) represents an east–west tilting mode in the tropical Pacific, typical of the mature phase of La Niña events with an anomalously shallow thermocline in the east, deep thermocline in the west and related easterly wind anomalies at the equator (Harrison and Larkin 1998). Minima of EOF1 time series (Fig. 6b) are indeed observed during the largest El Niño events during the past 50 years (1972, 1982, 1986 and 1997). As IOD events tend to co-occur with ENSO events, EOF1 also displays typical features of negative IOD events (Saji et al. 1999; Webster et al. 1999), i.e. positive SSLA in the eastern Indian Ocean along the coast of Java and Sumatra, and negative SSLA in the southwest Indian Ocean (Fig. 6a). IOD-related wind anomalies generate equatorial Kelvin waves, that further propagate northward as coastal Kelvin waves as they reach Java, explaining the in-phase SSLA variations along the

western rim of the Bay of Bengal, in agreement with observations (Rao et al. 2010). Finally, the positive signal that appears along the western coast of Australia is related to the variability in the western Pacific through coastal wave propagation in the Indonesian region (e.g. Clarke 1991; Wijffels and Meyers 2004; Feng et al. 2003).

The second interannual mode (Fig. 6c) involves a north–south tilting along an axis centred near 5°N, with a maximum of variability in the southwest Pacific. This second mode represents the recharge-discharge mode of warm waters in the equatorial region, described by Jin (1997). The equatorial recharge indeed leads the east–west tilting of the thermocline associated with El Niño events by about 8 months in the model (Fig. 6d vs. b), consistent with theory and lag correlations between NWP and SWP shown in Table 3. This second mode is associated with weaker SSLA and negligible wind signals in the Indian Ocean. The combination of the first two EOFs in the southern tropical Indian Ocean (strongly correlated at a lag of 8 months) also describes westward propagation of Rossby waves during and after IOD events.

The picture is somewhat different at decadal timescales (Fig. 6e–h). The first two modes explain 47 and 15 % of total variance respectively. In contrast to interannual timescales, there is less difference in the variance explained between the second and third mode that explains 11 % of the total signal. In the tropical Pacific, the first mode (Fig. 6e) is similar to the typical SLA pattern describing decadal variations of the subtropical cells (see Fig. 1 of LM08). The wind pattern of Fig. 6e indeed

induces a typical Kelvin upwelling–Rossby downwelling response. The geostrophic flow associated to these waves results in an increase of equatorward convergence of py-cnocline waters, i.e. a strengthening of the lower branch of the Pacific sub-tropical cells since the early 1990s (Fig. 6f, LM08) and a weakening before (Fig. 6f, McPhaden and Zhang 2002). This pattern is related to a sea level rise along the west Australian coast, consistent with the decadal variability in this region being forced remotely by winds in the tropical Pacific and transmitted via the Indonesian Archipelago (Feng et al. 2010), as for interannual time-scales. Interestingly, this first mode is neither related to SSLA anomalies nor to any wind signals anywhere else in the Indian Ocean. These results are in apparent contradiction with LM08, who revealed a near-coherent large-scale decadal variability in much of the Indo-Pacific region, with anti-correlated trade winds, SLA and sub-tropical cells variability at decadal timescales in the two oceans. This will be further discussed in the following section.

The second mode (Fig. 6g) displays smaller scale patterns as compared to the first mode. This mode shows decadal variations in the far western Pacific in the Min-danao dome region (Kashino et al. 2009), varying in phase with the west Australian and Indonesian coast. Opposite signals are found in the SWIO region. In contrast to the first mode, this Indo-Pacific SSLA pattern is associated with wind anomalies in both the Indian and Pacific Ocean, reminiscent of decadal modulation of the Walker circulation intensity: easterlies in the far western Pacific, and westerlies in the eastern equatorial and south tropical Indian Ocean. Depending on the period considered, the temporal evolution of the first two EOFs for decadal timescales can either vary in phase (as during the late 1990's where they both show a decrease), or vary in phase opposition (like at the end of the period).

4.3 Mechanisms of regional decadal variability

In this section, we discuss the possible driving mechanisms of decadal SSLA in each region. We chose not to present the same analysis for interannual variability, because it shows well-known ENSO and IOD patterns (and inter-basin connection between the western Pacific and WAC), which have been discussed in the previous section and elsewhere in literature (e.g. Landerer et al. 2008; Wijffels and Meyers 2004).

It suits to have a brief discussion on the expected dynamics at decadal timescales. Some of the concepts necessary to understand the response of an ocean basin to wind stress are laid-out in a seminal paper by Anderson and Gill (1975). This paper demonstrates that the typical adjustment time to attain the Sverdrup (1947) balance at any given point is the time it takes for planetary wave to
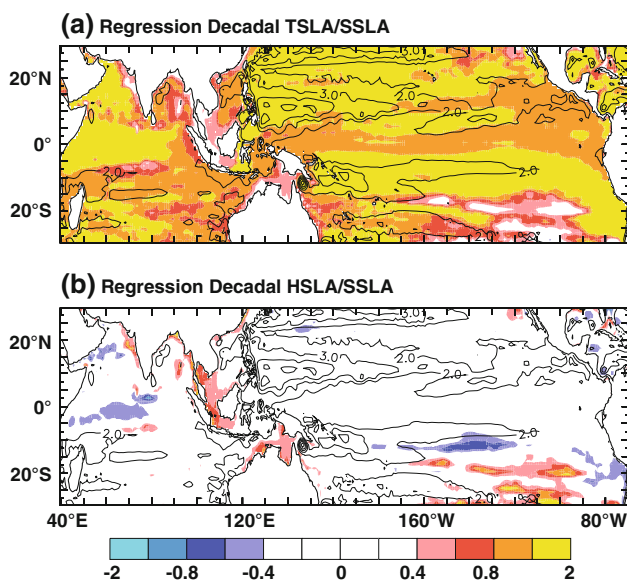
Fig. 5 Regression coefficients of model **a** thermosteric and **b** halosteric sea level to model steric sea level at decadal timescales. The standard deviation of decadal steric sea level is also shown by contours on each panel
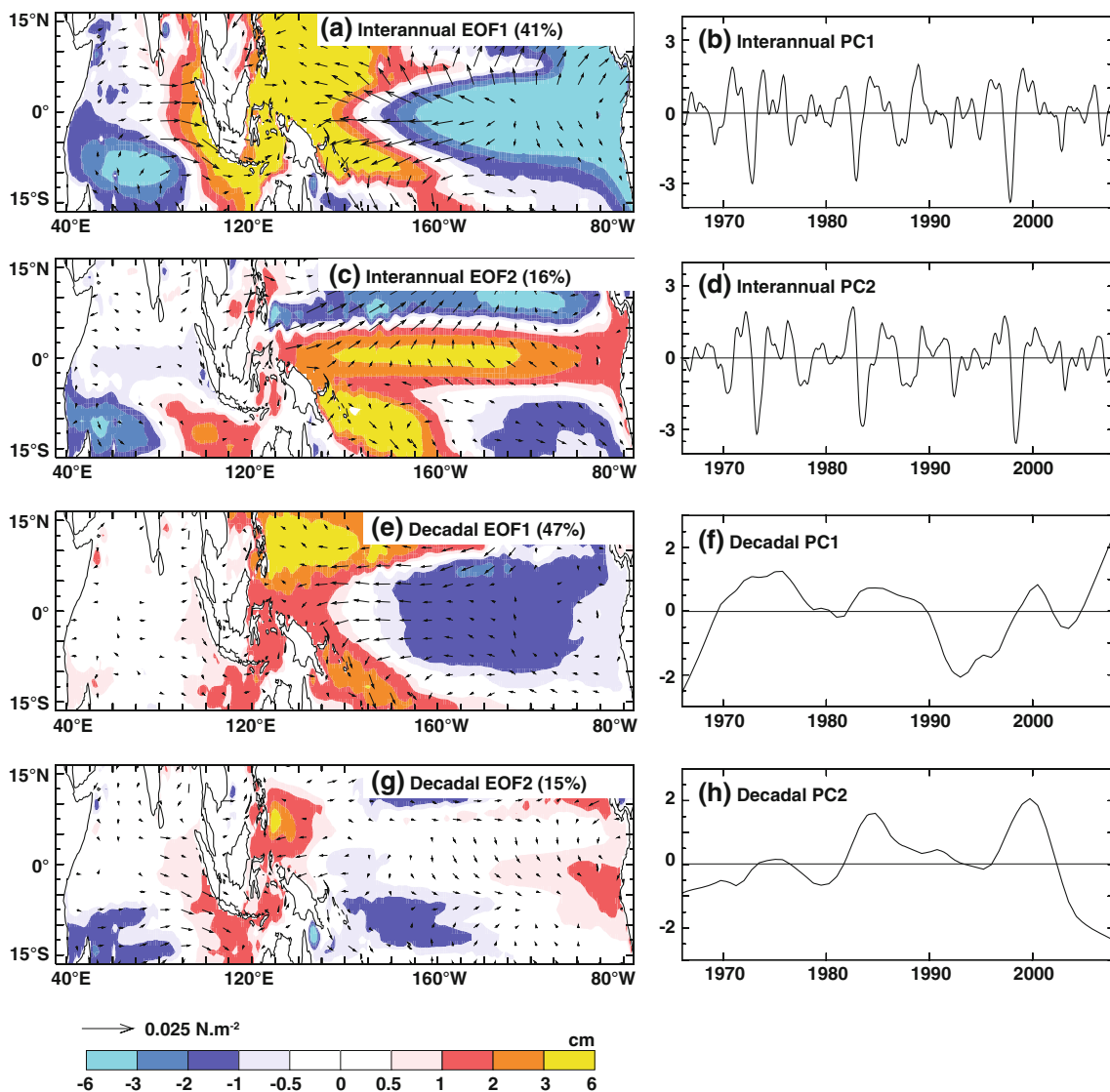
Fig. 6 First two EOF patterns of the model steric sea level anomalies over the Indo-Pacific sector (*left column*) and their corresponding normalized principal components (*right column*) at interannual (**a–d**) and decadal timescales (**e–h**). The *arrows* display the wind stress components regressed onto each normalized PCs. The percentage variance explained by each EOF is shown in *brackets*. Units are in cm for EOF patterns

reach this point from the boundary (or forcing region, in the case of non-uniform wind stress). Here, we focus on decadal sea level variations, i.e. variations with typical timescales longer than 7 years and focus on the tropical region (i.e. equatorward of 20° of latitude). A first baroclinic Rossby wave travels at $\sim$0.07 ms^{-1} at 20° of latitude (and faster equatorward). In 7 years, such waves will travel more than 15,000 km, leaving enough time to cross the entire Pacific or Indian ocean, in the whole tropics. At decadal timescales, we can hence consider that waves travel almost instantly: this is what being referred to as the "fast wave limit" in some studies (e.g. Neelin 1991). The Sverdrup balance can be rewritten to link the zonal sea level gradient with the curl of the wind stress away from

the equator and with the zonal wind stress at the equator. In the 'fast wave limit', we hence expect decadal sea level variations to be the result of upstream (i.e. to the east) wind stress curl variations away from the equator. At the equator, decadal sea level variations should be linked to zonally-averaged wind stress. Some regions, like the Bay of Bengal, are connected to the equatorial strip by a coastal waveguide (e.g. McCreary et al. 1996), and can also be influenced upstream by average equatorial zonal wind stresses in the Indian Ocean.

SSLA in NWP largely co-varies with SWP at decadal timescales, with a 0.71 correlation (Table 3). Decadal variations in the western tropical Pacific (NWP and SWP) are both strongly related to variations in equatorial easterlies
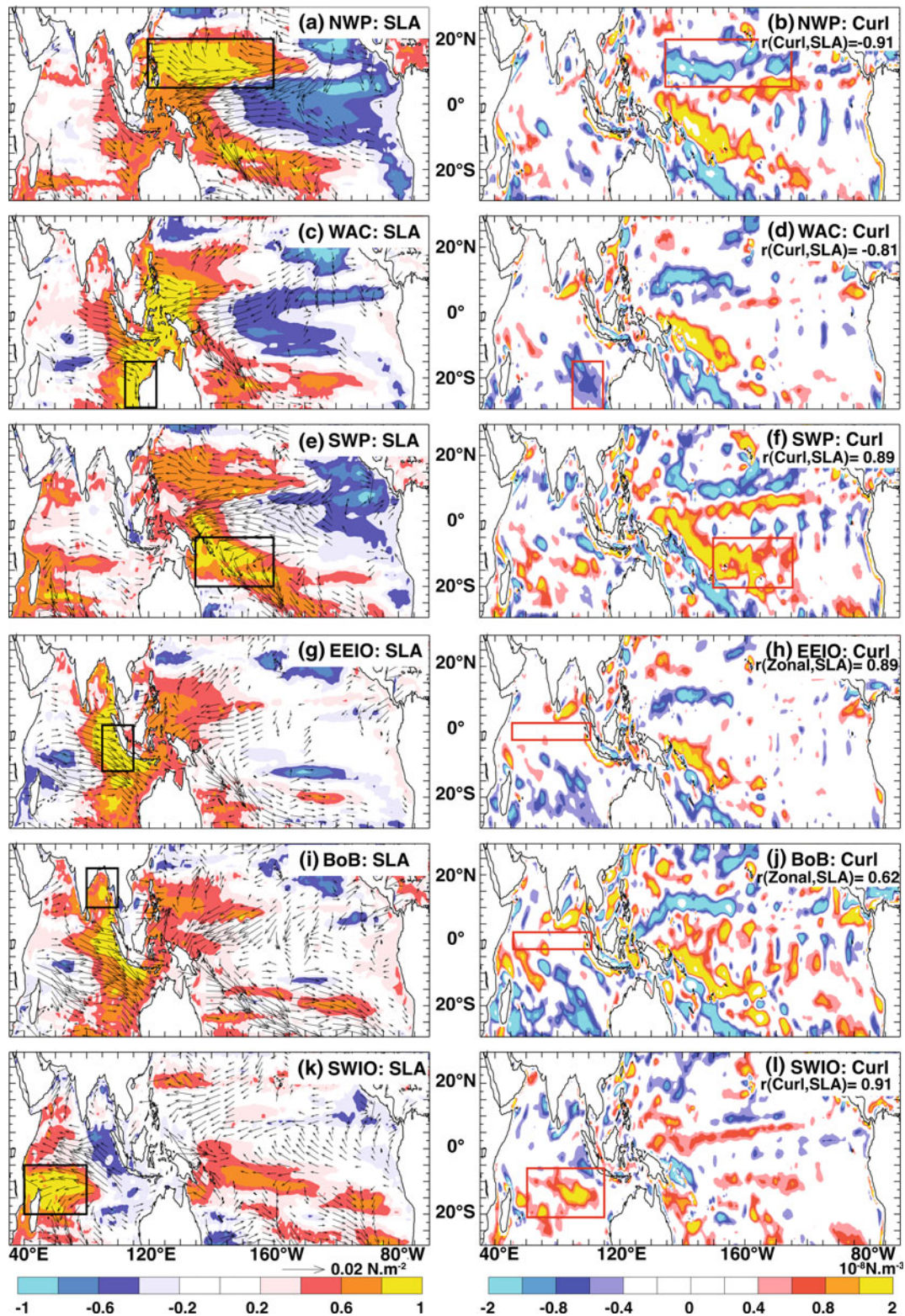
Fig. 7 a Correlation of model SSLA averaged over the NWP to the entire Indo-Pacific region (*color*) and regression of wind stress components (*arrows*) to the model normalized SSLA averaged over NWP. **b** Regression of wind stress curl to the normalized model SSLA averaged over NWP. Same for WAC (**c**, **d**), SWP (**e**, **f**), EEIO (**g**, **h**), BoB (**i**, **j**) and SWIO (**k**, **l**). The *numbers provided* below the title in the *right column* indicate the correlation coefficient between the average SSLA within the *black frame* (on the *left*) and average zonal wind stress (or wind stress curl) within the *red frame* (on the *right*)

Table 5 Correlation coefficient of wind stress variations at decadal time-scales between selected regions in the Indo-Pacific sector from different datasets

	Model	NCEP	Twentieth century	WASWind
Zonal(Pac)/Zonal(EIO)	−0.18	−0.10	0.08	−0.25
Zonal(Pac)/Curl(SIO)	0.23	0.21	−0.03	0.18
Zonal(EIO)/Curl(SIO)	−0.62	−0.76	−0.64	−0.56

Zonal(Pac) refers to the equatorial Pacific zonal wind stress (140°E–140°W; 2.5°N–2.5°S; red box on Fig. 8a), Zonal(EIO) to the equatorial Indian Ocean zonal wind stress (50°E–100°E; 2.5°N–2.5°S; green box on Fig. 8b) and curl(SIO) to south Indian Ocean wind stress curl (60°E–110°E; 20°S–5°S; yellow box on Fig. 8b)

(Figs. 7a, e). These SSLA patterns and associated wind structures are similar to those of the first EOF of Indo-Pacific decadal variations displayed in Fig. 6e, with rather weak wind signals in the Indian Ocean. These SSLA changes in the Pacific Ocean can easily be explained by upstream (i.e. to the east) wind changes. The northern flank of the equatorial easterly wind perturbation (Fig. 7a) is associated with negative wind stress curl (i.e. downwelling in the northern hemisphere; red box on Fig. 7b), east of the maximum SSLA perturbation in NWP. This is hence coherent with wind-driven downwelling, and westward propagation of SSLA through planetary waves. The same mechanism accounts for SSLA variations in the SWP, as the result of positive wind stress curl (downwelling in the southern hemisphere) on the southern flank of the easterly wind perturbation (Fig. 7e). Both NWP and SWP decadal SSLA variations are strongly correlated with wind stress curl variations to the east (r = −0.91 and 0.89 respectively; see Fig. 7), thus confirming qualitatively the Sverdrup balance at decadal timescales.

As indicated on Table 3, decadal SSLA along the WAC is correlated to decadal SSLA variations in the NWP (r = 0.64) and displays an even stronger correlation (r = 0.89) with SSLA within the Mindanao Dome region in the western equatorial Pacific (5°N–5°S; 120°E–160°E). WAC SSLAs are associated with a westerly wind signal in the eastern Indian Ocean and easterly wind signals in the western Pacific (Fig. 7a, c). The local wind signal in the Indian Ocean can however not explain the SSLA variations off the WAC, because this negative wind stress curl indeed induces upwelling in the southern Indian Ocean, and would hence drive a negative SSLA. In addition, the wind pattern is located westward of the maximum SSLA perturbation, which is not consistent with the westward propagation of SSLA signals by planetary waves. The signal at the WAC is hence linked to the upstream influence of the western Pacific through the Indonesian throughflow at decadal timescales (e.g. Feng et al. 2004, 2010). The dynamical arguments above suggest that those changes should be balanced by zonal wind stress changes in the equatorial Pacific. The 0.8 correlation between the SSLA in the WAC and zonal wind stress to the west of the dateline in the equatorial Pacific (not

shown) further supports this hypothesis. Local wind variations in the Indian ocean may however contribute to limit the westward expansion of remotely-driven decadal sea level variations at the WAC, as they will tend to counteract the Rossby wave signals radiated from the WAC region.

With the exception of WAC and BoB all other decadal signals in the Indian Ocean can directly be related to regional wind perturbations. EEIO and BoB decadal SSLA strongly co-vary (r = 0.86; Table 3) and are both strongly related to zonal wind variations over the central and eastern equatorial Indian Ocean (Fig. 7g, i). Equatorial westerly wind stress anomalies indeed generate downwelling Kelvin waves, which induce SSLA variations in the eastern equatorial Indian Ocean, and then propagate into the Bay of Bengal as coastal Kelvin waves, as observed at intra-seasonal (Vialard et al. 2009), seasonal (McCreary et al. 1996) and interannual (Rao et al. 2010) timescales. The strong correlation between the wind variations in the equatorial Indian Ocean and SSLA variations in the EEIO and BoB (r = 0.89 and 0.62 respectively) further support this hypothesis. Decadal variability in this region is not strongly related to variations in the western Pacific, with correlations between EEIO and NWP weaker than 0.5 at decadal timescales (Table 3).

Finally, in contrast to the variability at interannual timescales, SWIO SSLA variability stands out as largely independent from the north west Pacific variations (r = 0.08; Table 3) and to a lesser extent from the variations in other regions in the Indian Ocean, such as the EEIO (r = −0.42; Table 3). SSLA decadal variations in the SWIO are highly correlated (r = 0.91) with wind stress curl further east (Fig. 7l), hence suggesting a similar mechanism (wind stress curl forcing in the fast-wave limit) as in the NWP and SWP. In the model, the wind stress curl in the south Indian Ocean (SIO) is weakly (∼0.23; Table 5) correlated with Pacific equatorial decadal zonal wind stresses, hence explaining the weak connection between the SWIO and the western Pacific (r = 0.08; Table 3). The wind stress curl in the SIO is more related to EIO zonal wind stress anomalies but not entirely (r = −0.62). This is probably due to the fact that wind stress curl in the southern Indian Ocean is not only influenced by equatorial wind stress, but probably also by wind variations

Fig. 8 First two EOF patterns of the zonal wind stress over the Indo-Pacific sector at decadal timescale for (**a**, **b**) model forcing, (**c**, **d**) NCEP reanalysis, (**e**, **f**) twentieth century reanalysis and (**g**, **h**) WASWind product. The *arrows indicate* the wind stress components regressed onto the normalized PCs. The percentage variance explained by each EOF is shown in *brackets*. Units are in N m^{-2}
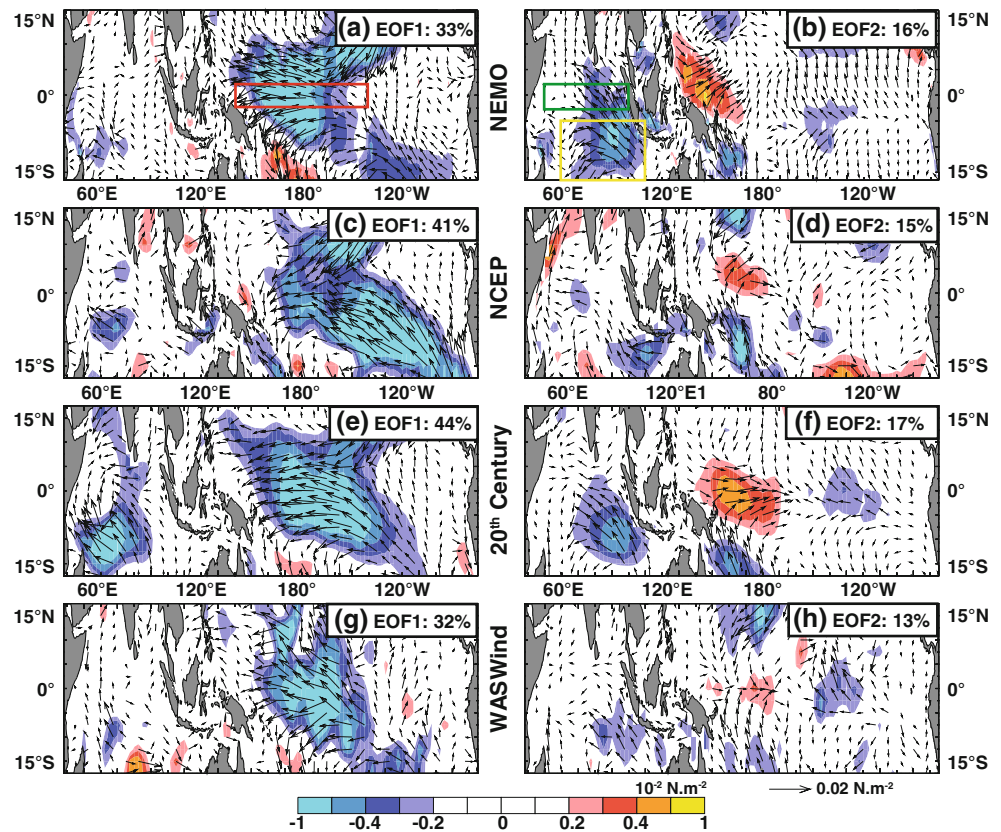
further south. This influence of extra-equatorial wind stress is hence explaining the relatively loose connection (r = −0.42; Table 3) between the SWIO and EEIO SSLA variability at decadal timescales.

4.4 Robustness of the decadal wind forcing

The results discussed so far have been obtained from the OGCM forced with ERA-40 derived wind stress. So, these results may however be highly dependent on the forcing wind product, as decadal wind variability may not be well constrained before the satellite era due to the scarcity of in situ near surface wind observations. Hence, we analysed decadal wind variability in the NCEP, twentieth century re-analyses and WASWind datasets over the model forcing period (1958–2007) to assess the robustness of the model results.

We first performed an EOF analysis to extract the main mode of wind decadal variability depicted by each dataset. The first EOF mode displays similar patterns in each of the products (Fig. 8). It explains between 32 % (WASWind dataset) and 44 % (twentieth century reanalysis) of the total variance and exhibits strong easterly wind anomalies in the central Pacific for all products. This wind pattern is reminiscent of the wind variations associated with model decadal SSLA in the NWP and SWP (Figs. 8a and 6e, whose associated principal components are correlated at

0.92). Despite this broad agreement in the Pacific, there is more discrepancy in the Indian Ocean. In the twentieth century reanalysis, south-easterly anomalies in the south-western Indian Ocean co-vary with the equatorial Pacific wind signal. This signal is considerably weaker in the three other datasets. The second mode of decadal wind variability also displays some similarities between the different datasets and explains between 13 % (WASWind) and 17 % (twentieth century reanalysis) of the total variance (right panel of Fig. 8). It consists of south-easterly wind anomalies in the south-eastern Indian Ocean combined with westerly wind anomalies in the far western Pacific. Although there are regional discrepancies, this simple EOF analysis reveals that the spatial structure of the decadal variability in the tropical Indo-Pacific region is relatively consistent amongst the different products analysed.

Mechanisms of decadal SSLA variability outlined in Sect. 4 stress the importance of wind variations in three key regions of the tropical Indo-Pacific sector. Zonal wind variations in the equatorial western Pacific largely drive decadal SSLA in the western Pacific and along the WAC. Zonal wind variations in the equatorial Indian Ocean drive decadal SSLA in the eastern equatorial Indian Ocean and the Bay of Bengal. Wind stress curl variations in the south Indian Ocean drive SSLA in the south–western Indian Ocean. Decadal wind variations in these three regions are
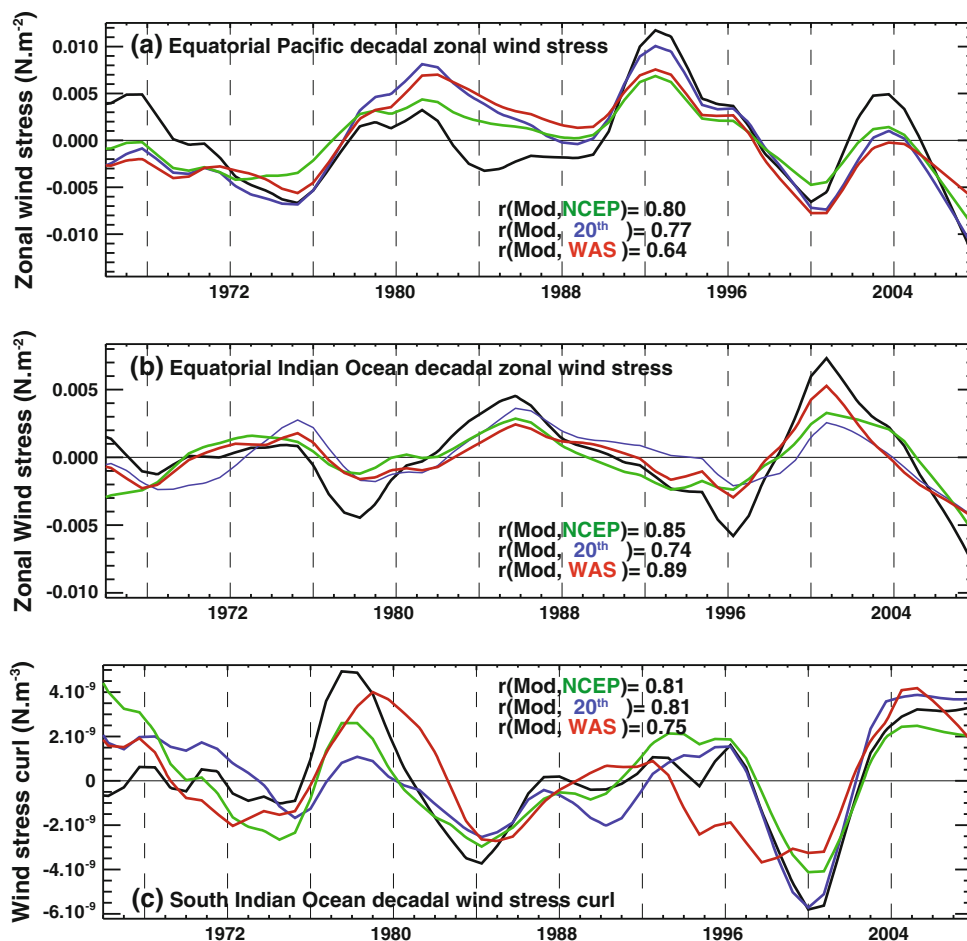
Fig. 9 Time series of decadal (**a**) equatorial Pacific zonal wind stress (140°E–140°W, 2.5°N–2.5°S; *red box* on Fig. 8a), **b** equatorial Indian Ocean zonal wind stress (60°E–100°E, 2.5°N–2.5°S; *green box* on Fig. 8b) and **c** south Indian Ocean wind stress curl (60°E–110°E, 20°S–5°S; *yellow box* on Fig. 8b) from model output (*black line*, similar to ERA40), NCEP reanalysis (*green line*), twentieth century reanalysis (*blue line*) and WASWind dataset (*red line*). The correlation coefficient between the model forcing and other datasets is indicated on each panel

displayed in Fig. 9, for the four datasets (model forcing, NCEP, Twentieth Century, WASWind). The four datasets show very coherent decadal zonal wind variations in the equatorial Pacific region (Fig. 9a), with local maxima in the early-70's, early-80's and early-90's and around 2004. Model wind variations have correlations with other products ranging from 0.64 (WASWind) to 0.80 (NCEP). Similarly, all wind datasets display very coherent decadal zonal wind fluctuations in the equatorial Indian Ocean (Fig. 9b), with local maxima in the mid-70's, mid-80's and around 2000 and correlation between the model forcing and other products ranging from 0.74 (twentieth reanalysis) to 0.89 (WASWind). The various datasets display as well coherent decadal wind stress curl variations in the South Indian Ocean, with local maxima in the early 60's, late 70's, early 90's and at the end of the record in all datasets. The model wind stress curl displays good correlations with other datasets (from 0.75 for WASWind to 0.81 for NCEP). In addition, the relationships between the three different

regions are quite consistent when comparing the different datasets, with weak correlations between the wind variability in the Pacific and the Indian Ocean and strong negative correlations in Indian Ocean between fluctuations of equatorial winds and wind curl in the south (Table 5). In the Indian Ocean, decadal zonal wind variations at the equator and decadal wind stress curl variations in the Southern hemisphere are moderately anti-correlated ($\sim r = -0.6$), while these two regions display very weak correlations with zonal wind variability in the equatorial Pacific region.

5 Long-term trends in the Indo-Pacific Ocean

5.1 Basin-scale pattern of long-term steric sea level trend

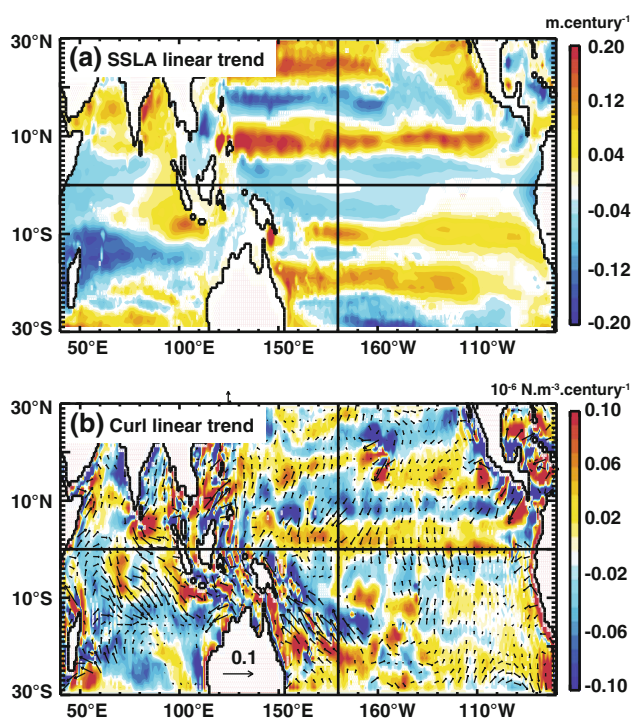SSLA trends in the Indian Ocean in Fig. 10a are similar to those from Timmermann et al. (2010) analysis using the

Fig. 10 Linear trend over the 1966–2007 period for (**a**) model steric sea level and **b** model wind stress curl (*in colors*). The vectors on panel **b** show the linear trend of model wind stress components. Units are m century^{-1} for steric sea level trend, N m^{3}century^{-1} for wind stress curl and N m^{-2} century^{-1} for wind stress

SODA ocean re-analysis. They are also similar to the modelling results from Han et al. (2010) and Timmermann et al. (2010). This is somewhat normal considering the fact that these studies also used ERA-40 to force their ocean models, as we did. SSLA has decreased substantially in the southwest Indian Ocean whereas it has increased elsewhere in the Indian Ocean (Fig. 10a). This decrease is also evident from Fig. 4k. This pattern is likely to be driven by surface wind changes. The trend of surface-wind stress pattern shows an enhanced convergence around 15°S owing to the anomalous north-westerly winds from the equator (Fig. 10b). These wind changes result in a large negative wind stress curl anomaly around 10°S in the Indian Ocean, dynamically consistent with the SSLA decrease observed in the South-western Indian Ocean region.

In the Pacific, zonally oriented bands of alternating sign SSLAs characterize the long term SSLA trend. This SSLA trend is also dynamically consistent with the linear trend in wind stress, being qualitatively consistent with the alternating bands of positive and negative curl and associated Ekman convergence/divergence. The SSLA trend in the Pacific Ocean does not agree as well with the results of Timmermann et al. (2010) as in the case of the Indian Ocean. There is a very broad agreement, but exhibits strong differences along two bands at 10°S and 15°N. We will

discuss possible sources of those differences in the following section.

5.2 Robustness of the wind forcing trends

In this section, we assess the robustness of the model SSLA long-term trends in the Pacific and Indian oceans by evaluating the sensitivity of the wind forcing trend estimate to various wind products (model forcing, WASWind, NCEP, twentieth century) and to the trend estimation period.

Figure 11 shows regional long-term trends in the four wind datasets. While wind stress decadal variations are rather consistent (Sect. 4.4), it is not the case for the long-term linear trends. While the model forcing exhibits a significant negative Ekman pumping signal in the southern Indian Ocean between 30°S and 10°S, trends are very different in the other datasets. The twentieth century reanalysis displays a positive Ekman pumping anomaly south of 10°S and a negative Ekman pumping anomaly further north (with a minimum around 5°S). NCEP displays a positive Ekman pumping anomaly north of 20°S. When averaging between 20°S and 5°S (where largest SSLA trends are found in the south-western Indian Ocean, Fig. 10a), it appears that the model dataset is showing a significant negative trend (consistent with the SSLA decrease in this region), while NCEP is showing a positive curl trend and the two other datasets showing no significant trends. Similarly, Indian Ocean equatorial zonal wind stress linear trends largely differ in the various datasets (Fig. 11b): the model displays a significant positive zonal wind stress trend all over the equatorial region, WASWind exhibits a negative trend while NCEP and twentieth century reanalysis show latitude bands where trend is alternatively positive and negative. When averaged within the equatorial waveguide, results also strongly vary depending on the wind product considered: the model displays a positive trend, while other products display weak or insignificant changes. Wind products exhibit similar trend discrepancies in the Pacific, with opposite signs for the averaged trends of north Pacific wind stress curl (Fig. 11c) and equatorial Pacific zonal wind stress (Fig. 11d). The only region where the trend is reasonably consistent amongst the datasets is the South Pacific where three of the products display a negative trend, consistent with the SSLA decrease discussed in Timmermann et al. (2010).

Trend estimation is not only sensitive to the dataset used but also to the period considered to estimate the trends. Figure 12 provides the average wind stress curl trend estimate in the South Indian Ocean and South Pacific as a function of the starting date (with the trend computation period varying from 1958–2007 to 1978–2007). In the South Indian Ocean (Fig. 12a), while NCEP and the model forcing exhibit a consistent wind stress curl trend for the
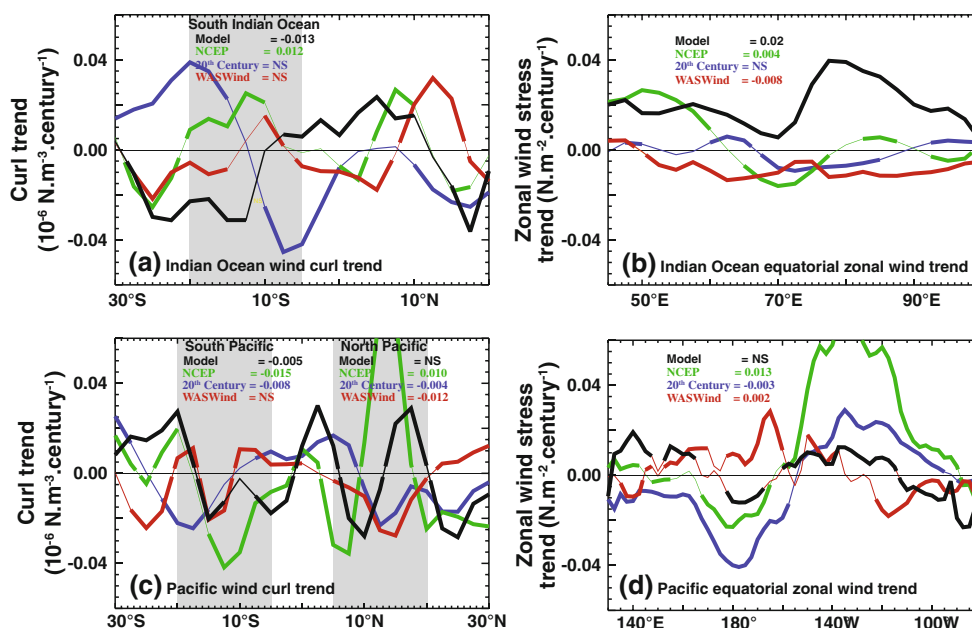
Fig. 11 a Zonal average wind stress curl linear trend over the Indian Ocean (60°E–110°E) over the 1966–2007 period for the four datasets considered (twentieth century reanalysis, NCEP, WASWind and model). Average wind stress curl linear trend in the South Indian Ocean (20°S–5°S) is also indicated for each dataset. **b** 2.5°N–2.5°S averaged zonal wind stress linear trend over the 1966–2007 period in the Indian Ocean. Average zonal wind stress linear trend in the Equatorial Indian Ocean is also indicated for each dataset. **c** Same as (**a**) but in the Pacific (160°E–120°W). Average wind stress curl linear trend in the North (5°N–20°N) and South Pacific (20°S–5°S) is also indicated for each dataset. **d** Same as (**b**) but in the equatorial Pacific. Average zonal wind stress linear trend in the Equatorial Pacific is also indicated for each dataset. Units are N m^{-3} century^{-1} for wind stress curl and N m^{-2} century^{-1} for wind stress. *Bold lines* indicate trends that are significantly different from zero at 95 % confidence level

range of periods considered (positive for NCEP, negative for the model), trends estimation for WASWind product and the twentieth century reanalysis vary depending on the estimation period, being either negative if the starting date to calculate the trend is chosen before 1966 or insignificant or positive if the starting date is chosen after 1966. Results are more coherent for the South Pacific where three datasets (model forcing, twentieth century and NCEP reanalysis) show a consistent negative wind stress curl if the starting date to calculate the trend is chosen before 1974 while the WASWind trend generally remains insignificant. We obtain similar discrepancies amongst products by also varying the end-date, or by changing the box definition (not shown). This indicates that long-term trends are not as consistent as decadal variations of the wind stresses by current re-analysis products.

6 Conclusion

6.1 Summary

In this study, we investigate decadal steric sea level variations and long-term trends in the Indo-Pacific sector using results from an OGCM simulation over the 1966–2007 period. The simulation compares favourably with sea level from satellite altimetry (after 1993) and available tide gauges in the Indo-Pacific region. The largest decadal variations occur in the Northwest and Southwest Pacific, along the coast of Java and Sumatra, in the Bay of Bengal, along the West Australian coast and south–western Indian Ocean. In these regions, interannual variations (up to 10 cm standard deviation in the western Pacific) are two to three times larger than the decadal ones (up to 5 cm in the western Pacific), while the linear trend over the full record is about two to three times smaller than decadal variations (up to 2 cm in the northwest Pacific and south-western Indian Ocean). Regions of largest decadal variations coincide with regions of strong interannual variability, with the noticeable exception of the eastern equatorial Pacific that displays a clear maximum of interannual variability linked to ENSO, but little decadal variability.

As already discussed by several authors (Qiu and Chen 2006; LM08, Timmermann et al. 2010; Han et al. 2010), the results of this study confirmed that wind variations largely explain the sea level variability at decadal and multidecadal time-scales in the tropical Indo-Pacific sector. Large-scale patterns of decadal variability involve variations of the easterlies in the central and western Pacific Ocean, and of the westerlies in the equatorial and south Indian Ocean.
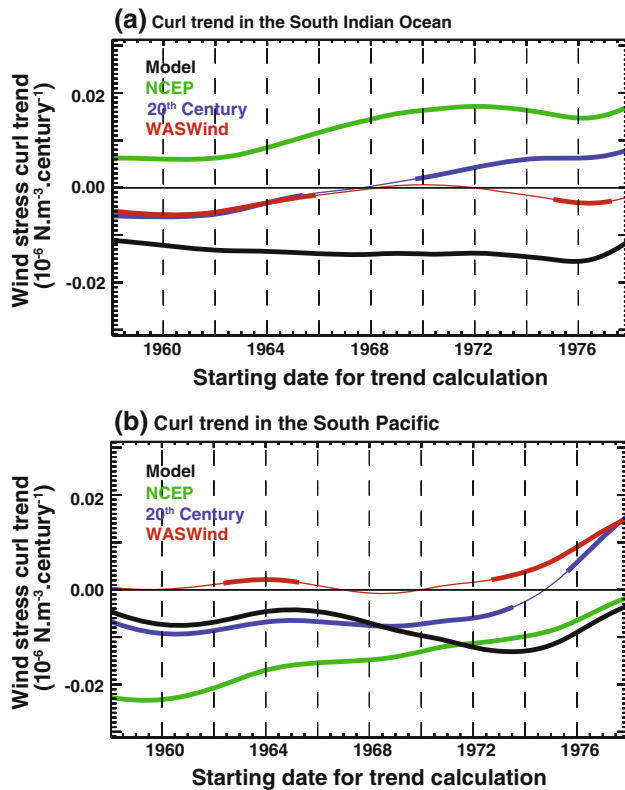
Fig. 12 Linear trend of the wind stress curl averaged over (**a**) the south Indian Ocean (60°E–110°E, 20°S–5°S) and **b** the south Pacific (160°E–120°W, 20°S–5°S) for the four wind datasets considered (twentieth century reanalysis, NCEP, WASWind and model), as a function of the starting date of the trend computation period (with this period varying from 1958–2007 to 1978–2007). The *bold lines* indicate when the trend is significantly different from zero at the 95 % confidence level

Those zonal winds decadal variations are relatively independent of each other in the Indian and Pacific Oceans, in contrast to variations at interannual timescales, which are clearly linked through the tendency of ENSO and the IOD to co-occur. The strong decadal wind stress curl fluctuations on the northern and southern flanks of the western Pacific force Rossby waves, responsible for decadal variations in the northwest and southwest Pacific regions. Oceanic teleconnections transmit this signal from the western Pacific to the west Australian coast, through equatorial and coastal waveguides. This results the decadal variability along the WAC that varies in phase with that in the western Pacific, in a similar way to what happens at interannual timescales (correlation around 0.7 for both timescales over 1966–2007). These results confirm the strong relationship between these two regions at interannual timescales (e.g. Clarke 1991; Wijffels and Meyers 2004; Feng et al. 2005), but also the observational analysis from tide gauge data performed by Feng et al. (2010) at decadal timescales.

In the Indian Ocean, our results further reveal the modulation of the strength of the equatorial trade winds

that drive Kelvin waves, propagate to the eastern equatorial Indian Ocean and Bay of Bengal through the equatorial and coastal wave guides. As a result, the SSLA variations in these two regions are highly correlated at (r = ∼0.8) at both interannual and decadal timescales. While Rao et al. (2010) discussed this connection using satellite data for interannual timescales, it had not been reported earlier for decadal timescales. Ekman pumping variations south of the equator in the Indian Ocean, drive planetary waves that induce decadal sea level variations in the southwest Indian Ocean. Interannual variations of SSLA in the southwest Indian Ocean, encompassing Seychelles-Chagos thermocline ridge, have a -0.7 correlation with those in the eastern equatorial Indian Ocean but this correlation considerably weakens (−0.4) at decadal timescales. This weaker association at decadal timescales probably comes from the fact that the strength of equatorial easterlies is not the only factor controlling the Ekman pumping south of the equator at decadal timescales. In addition, decadal steric sea level variations in the south-western and to a lesser extent in the eastern equatorial Indian Ocean are independent of decadal variations in the northwest Pacific in agreement with the independency found in the decadal wind forcing over the Indian and Pacific sector.

In agreement with Timmermann et al. (2010), most of the steric sea level decadal signals in our model experiment are dynamically consistent with wind stress forcing. We have hence investigated the robustness of the decadal wind stress forcing in our model by comparing it with three other products (WASWind product, NCEP and twentieth century reanalysis). The large-scale wind forcing patterns in those products are consistent, as well as the decadal wind evolution in key regions (zonal winds in the western and central Pacific, zonal winds in the equatorial Indian ocean and wind stress curl in the Southern Indian Ocean). The relationships between these decadal wind variations are also very consistent amongst these products, with an independency between the decadal variability in the Indian Ocean and the Pacific sector.

Decadal and interannual SSLA variability share a lot of common features such as strong variability in the western Pacific, along the coast of Java and Sumatra, in the Bay of Bengal, along the west Australian coast and south-western Indian Ocean. There is a strong co-variability between the western Pacific and the west Australian coast and between the eastern equatorial Indian Ocean and the Bay of Bengal through equatorial and coastal waveguides with similar forcing mechanisms at interannual and decadal timescales. There are also noticeable differences between interannual and decadal steric sea level variability such as a weaker amplitude of SSLA at decadal period compared to interannual variability, a weaker association of the Pacific and Indian ocean winds at decadal timescales, no noticeable

SSLA variability in the eastern equatorial Pacific at decadal timescales and a weaker association between the eastern equatorial and south-western Indian ocean steric sea level at decadal timescales.

Regarding the long-term linear trend of SSLA over the 1966–2007 period, our results agree with previous findings of Han et al. (2010) and Timmermann et al. (2010). SSLA decreases substantially in the south-western Indian Ocean, in response to a large negative wind stress curl trend south of the equator whereas it increases elsewhere in the Indian Ocean. In the Pacific, zonally oriented bands of alternating signs, dynamically consistent with the curl linear trend, characterize the long-term sea level trend. The very broad agreement with the results of Han et al. (2010) and Timmermann et al. (2010) is not surprising, as the wind forcing used in these studies is similar to one used in our simulation (ERA40). However, comparison of our model wind forcing with other products reveal a very strong dependence of the long-term wind stress trend to the wind product as well as a moderate dependence to the length of the period over which the trend is estimated. This suggests that estimates of long-term trends in sea level from forced ocean models need to be interpreted with caution.

6.2 Discussion and perspectives

In this section, we first discuss limitations inherent to the approach in our study, and then discuss our results in the context of other recent studies about decadal and multi-decadal variability of the Indo-Pacific Ocean. We finally discuss the perspectives evolved from the current study.

The time span of the OGCM experiment discussed in this study (1966–2007, i.e. 42 years) is short since we investigate the variability at time scales of ~ 7 years and longer. Obviously, the number of degrees of freedom in our dataset is low (≤ 5), as well as the statistical significance of correlations that we provide. Whereas some confidence is provided by the dynamical consistency of the simple physical mechanisms that we propose, the association between steric sea level variability in various regions in this study will hence need further verifications. An alternative method to check the sea level tele-connections and associated mechanisms would be to run sensitivity experiments with decadal variability applied in only specific regions. Experiments using only decadal wind stress variability and neglecting the freshwater and heat flux forcing decadal variations would also allow ascertaining the dominance of the dynamic forcing mechanism, over forcing by buoyancy fluxes. Finally, because of uncertainties in decadal and longer steric sea level variations, it would be interesting to run a series of experiments forced with various existing forcing products. This would allow investigating the full dynamical response of SSLA to uncertainties in the forcing product in a more thorough way than what we did in this study.

Feng et al. (2010) also described decadal sea level variations along the western Australian coast. They suggested a tele-connection through the equatorial and coastal waveguide in the Indonesian throughflow, similar to what is described at interannual timescales (Clarke 1991; Clarke and Liu 1993; Meyers 1996; Masumoto and Meyers 1998; Potemra 2001; Potemra et al. 2002; Wijffels and Meyers 2004; Cai et al. 2005a, b; Feng et al. 2003, 2005). The results from the present study are fully consistent with Feng et al. (2010). On the other hand, our results appear to contradict LM08 who underlined strong basin-scale connection between Pacific and Indian Ocean wind and sea level decadal variability. Indeed, apart from the western Australian coast region discussed above, we find that variability in other regions of the Indian Ocean seems to be relatively independent from the one in the Pacific. Over the 1993–2006 period, studied by LM08, the principal components describing the sea level variations over both basins (Fig. 6e–h) are largely in phase, with a phase change in 2000, consistent with LM08. This tendency considerably weakens over the entire 1966–2007 period (Fig. 4a, e; Table 3). We hence believe that the in-phase wind and related sea level variations between the Indian and Pacific oceans is not a general feature of decadal variations in those basins.

The results also slightly differ from those of Schwarz-kopf and Böning (2011), who suggest the influence of Pacific remote forcing on the SWIO region (their Figs. 2, 3, 4) using sensitivity experiments based on a very close numerical setup to the one that we use. This may be due to the fact that they do not explicitly separate decadal variability from interannual variability, and mostly focus on the multi-decadal variability (the "trend"). Looking at their results in more details (their Figs. 3, 4) suggest that, at decadal timescales, the variability in the SWIO is also dominated by regional forcing in the Indian Ocean, while the Pacific influence takes over at longer (multi-decadal) timescales.

The model SSLA shows a negative trend of steric sea level over 1966–2007 in the southern Indian Ocean, consistent with Han et al. (2010) and Timmermann et al. (2010), who used the same forcing (ERA40) on different periods (1958–2001 and 1961–2001 respectively). We agree with those two studies in attributing this sea level decrease to long-term changes in wind stress curl in the southern Indian Ocean, while Alory et al. (2007) attributed it to oceanic tele-connections with the Pacific Ocean. In the Pacific Ocean, our results differ more from those of Timmermann et al. (2010), who showed a ~ 20 cm per century sea level decrease in the western Pacific between 15°S and 5°S. When not considering the end of the record (i.e.

1966–2001 instead of 1966–2007), the steric sea level trends in our model is more consistent with Timmermann et al. (2010, not shown). This underlines once again that one must be very cautious when discussing multi-decadal wind stress variability. Indeed, as shown in Sect. 5.2, different products display quite different long-term trends in equatorial zonal wind stress, and wind stress curl (the main driving factors of long-term sea level variations). In addition, the moderate sensitivity of wind stress (and resulting sea level) variations in the considered period, demonstrated in Sect. 5.2, can become larger when looking at details of the spatial structure, as shown in Fig. 10. This confirm that the analysis of spatial patterns of long-term changes in sea level from forced ocean simulations must be taken with great care.

The fifth assessment report (AR5) of the Intergovernmental Panel on Climate Change (IPCC) (due in 2013) will make extensive use of the Coupled Model Inter-comparison Project 5 (CMIP5) experiments. This project will include both the usual long-term projections and also 'near term' (i.e. decadal) hindcasts and predictions, with an initialized ocean state starting every fifth year from 1960 to 2005 (Taylor et al. 2012). Those datasets will hence allow evaluating the inherent capacity of CMIP5 models to reproduce observed patterns of Indo-Pacific sea level decadal variations (long-term experiments), but also the ability of those models to predict the observed evolution of those patterns over recent decades (say 1970–2010). This pragmatic "forecast capacity evaluation" approach should however be completed by experiments trying to assess the predictability of Indo-Pacific decadal sea level variations in an idealized model context (i.e. with a most perfect model and perfect initial state, in order to evaluate decadal predictability upper limits given the influence of atmospheric stochastic forcing).

References

Alory G, Wijffels S, Meyers G (2007) Observed temperature trends in the Indian Ocean over 1960–1999 and associated mechanisms. Geophys Res Lett 34(2):L02606

Anderson DLT, Gill AE (1975) Spin-up of a stratified ocean, with applications to upwelling. Deep Sea Res 22:583–596

Antonov JI, Levitus S, Boyer TP (2002) Steric sea level variations during 1957–1994: importance of salinity. J Geophys Res 107(C12):8013

Barnier B, Madec G, Penduff T, Molines JM, Treguier AM, Le Sommer J, Beckmann A, Biastoch A, Böning C, Dengg J, Derval C, Durand E, Gulev S, Remy E, Talandier C, Theetten S, Maltrud M, McClean J, De Cuevas B (2006) Impact of partial steps and momentum advection schemes in a global ocean circulation model at eddy permitting resolution. J Ocean Dyn 56:543–567

Bindoff NL, Willebrand J, Artale V, Cazenave A, Gregory J, Gulev S, Hanawa K, Quéré C, Levitus S, Nojiri Y, Shum C, Talley L, Unnikrishnan A (2007) Climate change 2007: the physical science basis. Contribution of working group I to the fourth assessment report of the intergovernmental panel on climate change, chapter 5. Cambridge University press, Cambridge, pp 385–432

Blanke B, Delecluse P (1993) Variability of the tropical Atlantic ocean simulated by a general circulation model with two different mixed layer physics. J Phys Oceanogr 23:1363–1388

Brodeau L, Barnier B, Treguier A, Penduff T, Gulev S (2010) An ERA40-based atmospheric forcing for global ocean circulation models. Ocean Modell 31:88–104

Cai W, Hendon HH, Meyers G (2005a) An Indian Ocean dipole in the CSIRO coupled climate model. J Clim 18:1449–1468

Cai W, Meyers G, Shi G (2005b) Transmission of ENSO signal to the Indian Ocean. Geophys Res Lett 32:L05616

Cai W, Sullivan A, Cowan T (2008) Shoaling of the off-equatorial south Indian Ocean thermocline: is it driven by anthropogenic forcing? Geophys Res Lett 35:L12711

Carton JA, Giese BS, Grodsky SA (2005) Sea level rise and the warming of the oceans in the Simple Ocean Data Assimilation (SODA) ocean reanalysis. J Geophys Res 110:C09006

Cazenave A, Nerem RS (2004) Present-day sea level change: observations and causes. Rev Geophys 42:RG3001

Chelton DB, Schlax MG (1996) Global observations of oceanic Rossby waves. Science 272:234–238

Cheng X, Qi Y, Zhou W (2008) Trends of sea level variations in the Indo-Pacific warm pool. Global Planet Change 63:57–66

Church JA, Godfrey JS, Jackett DR, McDougall TJ (1991) A model of sea level rise caused by ocean thermal expansion. J Clim 4:438–444

Clarke AJ (1991) On the reflection and transmission of low-frequency energy at the irregular western Pacific Ocean boundary. J Geophys Res 96:3289–3305

Clarke AJ, Liu X (1993) Observations and dynamics of semiannual and annual sea levels. J Phys Oceanogr 23:386–399

Clarke AJ, Liu X (1994) Interannual sea level in the northern and eastern Indian Ocean. J Geophys Res 99:1224–1235

Cleveland RB, Cleveland WS, McRae JE, Terpenning I (1990) STL: a seasonal-trend decomposition procedure based on Loess. J Off Stat 6:3–73

Compo GP et al (2011) The twentieth century reanalysis project. Q J Roy Meteorol Soc 137:1–28

Cravatte S, Picaut J, Eldin G (2003) Second and first baroclinic Kelvin modes in the equatorial Pacific at intraseasonal timescales. J Geophys Res 108(C8):3266. doi:10.1029/2002JC001511

Cravatte S, Madec G, Izumo T, Menkes C, Bozec A (2007) Progress in the 3-D circulation of the eastern equatorial Pacific in a climate ocean model. Ocean Model 17:28–48

Durand F, Shankar D, Birol F, Shenoi SSC (2009) Spatio-temporal structure of the East India Coastal current from satellite altimetry. J Geophys Res 114:C02013

Feng M, Meyers G, Pearce A, Wijffels S (2003) Annual and interannual variations of the Leeuwin current at 32S. J Geophys Res 108(C11):3355

Feng M, Li Y, Meyers G (2004) Multi-decadal variations of Fremantle sea level: footprint of climate variability in the tropical Pacific. Geophys Res Lett 31:L16302

Feng M, Wijffels S, Godfrey S, Meyers G (2005) Do eddies play a role in the momentum balance of the Leeuwin Current? J Phys Oceanogr 35:964–975

Feng M, McPhaden MJ, Lee T (2010) Decadal variability of the Pacific subtropical cells and their influence on the southeast Indian Ocean. Geophys Res Lett 37:L09606

Greatbatch RJ (1994) A note on the representation of steric sea level in models that conserve volume rather than mass. J Geophys Res 99:12767–12771

Gregory JM (1993) Sea level changes under increasing atmospheric CO_2 in a transient coupled ocean-atmosphere GCM experiment. J Clim 6(12):2247–2262

Han W (2005) Origins and dynamics of the 90-day and 30–60-day variations in the equatorial Indian Ocean. J Phys Oceanogr 35:708–728

Han W, Meehl GA, Rajagopalan B, Fasullo JT, Hu A, Lin J, Large WG, Wang J, Quan XW, Trenary LL, Wallcraft A, Shinoda T, Yeager S (2010) Patterns of Indian Ocean sea level change in a warming climate. Nat Geosci 3:546–550

Harrison DE, Larkin NK (1998) El Niño-southern oscillation sea surface temperature and wind anomalies 1946–1993. Rev Geophys 36(3):353–399

Jackett DR, McDougall TJ (1995) Minimal adjustment of hydrographic profiles to achieve static stability. J Atmos Ocean Technol 12(4):381–389

Jin FF (1997) An equatorial ocean recharge paradigm for ENSO. Part I: conceptual model. J Atmosph Sci 54:811–829

Kalnay E et al (1996) The NCEP/NCAR 40-year reanalysis project. Bull Am Meteorol Soc 77(3):437–471

Kashino Y, Espana N, Syamsudin F, Richards KJ, Jensen T, Dutrieux P, Ishida A (2009) Observations of the north equatorial current, Mindanao current and the Kuroshio current system during the 2006/07 El Nino and 2007/08 La Nina. J Oceanogr 65:325–333

Keerthi MG, Lengaigne M, Vialard J, Montegut CB, Muraleedharan PM (2012) Interannual variability of the tropical Indian Ocean mixed layer depth. Clim Dyn. doi:10.1007/s00382-012-1295-2

Knapp KR, Kruk MC, Levinson DH, Diamond HJ, Neumann CJ (2010) The international best track archive for climate stewardship (IBTrACS): unifying tropical cyclone best track data. Bull Am Meteorol Soc 91:363–376

Landerer FW, Jungclaus JH, Marotzke J (2008) El Nino–Southern Oscillation signals in sea level, surface mass redistribution, and degree-two geoid coefficients. J Geophys Res 113:C08014

Lee T, McPhaden MJ (2008) Decadal phase change in large-scale sea level and winds in the Indo-Pacific region at the end of the 20th century. Geophys Res Lett 35:L01605

Lengaigne M, Vecchi GA (2009) Contrasting the termination of moderate and extreme El Niño events in coupled general circulation models. Clim Dyn 35:299–313

Lengaigne M, Madec G, Menkes C, Alory G (2003) Impact of isopycnal mixing on the tropical ocean circulation. J Geophys Res 108(C11):0148–0227

Lengaigne M, Boulanger JP, Menkes C, Spencer H (2006) Influence of the seasonal cycle on the termination of El Nino events in a coupled general circulation model. J Clim 19:1850–1868

Lengaigne M, Haussman U, Madec G, Menkes C, Vialard J, Molines JM (2012) Mechanisms controlling warm water volume inter-annual variations in the equatorial Pacific: diabatic versus adiabatic processes. Clim Dyn 38:1031–1046

Levitus S, Boyer TP, Conkright ME, O'Brien T, Antonov J, Stephens C, Stathoplos L, Johnson D, Gelfeld R (1998) NOAA Atlas NESDIS 18 and World ocean database, vol 1. U.S. Gov. Printing Office, Washington DC

Llovel W, Guinehut S, Cazenave A (2010) Regional and interannual variability in sea level over 2002–2009 based on satellite altimetry, Argo float data and GRACE ocean mass. Ocean Dyn 60:1193–1204

Madec G (2008) "NEMO ocean engine". Note du Pole de modéli-sation, vol 27. Institut Pierre-Simon Laplace (IPSL), France, pp 1288–1619

Masumoto Y, Meyers G (1998) Forced Rossby waves in the southern tropical Indian Ocean. J Geophys Res 103:27589–27602

McCreary JP, Kundu PK, Molinari RL (1993) A numerical investigation of dynamics, thermodynamics and mixed layer processes in the Indian Ocean. Prog Oceanogr 31:181–244

McCreary JP, Han W, Shankar D, Shetye SR (1996) Dynamics of the east India coastal current 2. Numerical solutions. J Geophys Res 101:13993–14010

McPhaden MJ (1999) Genesis and evolution of the 1997–1998 El Nino. Science 283:950–954

McPhaden MJ, Zhang DX (2002) Slowdown of the meridional overturning circulation in the upper Pacific Ocean. Nature 415:603–608

McPhaden MJ, Zhang D (2004) Pacific Ocean circulation rebounds. Geophys Res Lett 31(18):0094–8276

McPhaden MJ, Zebiak SE, Glantz MH (2006) ENSO as an integrating concept in earth science. Science 314:1740

Meehl GA et al (2009a) Decadal prediction: can it be skillful? Bull Am Meteorol Soc 90:1467–1485

Meehl GA, Aixue H, Benjamin DS (2009b) The mid-1970s climate shift in the Pacific and the relative roles of forced versus Inherent decadal variability. J Clim 22(3):780

Meinen CS, McPhaden MJ (2000) Observations of warm water volume changes in the equatorial Pacific and their relationship to El Niño and La Niña. J Clim 13:3551–3559

Meyers G (1996) Variation of the Indonesian through flow and the El Nino Southern Oscillation. J Geophys Res 101:12255–12263

Millero FJ, Poisson A (1981) International one-atmosphere equation of state of seawater. Deep-Sea Res 28:625–629

Mitas CM, Clement A (2005) Has the Hadley cell been strengthening in recent decades? Goephys Res Lett 32:L03809

Neelin D (1991) The slow sea surface temperature mode and the fast-wave limit: analytic theory for tropical interannual oscillations and experiments in an hybrid coupled model. J Atm Sci 48:584–606

Oliver ECJ, Thompson KR (2010) Madden-Julian Oscillation and sea level: local and remote forcing. J Geophys Res 115:C01003

Pattullo J, Munk W, Revelle R, Strong E (1955) The seasonal oscillation in sea level. J Mar Res 14:88–156

Paulson CA, Simpson JJ (1977) Irradiance measurements in the upper ocean. J Phys Oceanogr 7:952–956

Potemra JT (2001) Contribution of equatorial Pacific winds to southern tropical Indian Ocean Rossby waves. J Geophys Res 106:2407–2422

Potemra JT, Hautala SL, Sprintall J, Pandoe W (2002) Interaction between the Indonesian seas and the Indian Ocean in observations and numerical models. J Phys Oceanogr 32:1838–1854

Qiu B, Chen S (2006) Decadal variability in the large-scale sea surface height field of the south Pacific Ocean: observations and causes. J Phys Oceanogr 36:1751–1762

Rao AS, Behera SK (2005) Subsurface influence on SST in the tropical Indian ocean: structure and interannual variability. Dyn Atmos Oceans 39:103–135

Rao RR, Girish Kumar MS, Ravichandran M, Rao AR, Gopalakrishna VV, Thadathil P (2010) Interannual variability of Kelvin wave propagation in the wave guides of the equatorial Indian Ocean, the coastal Bay of Bengal and the Southeastern Arabian Sea during 1993–2006. Deep-Sea Res I 57:1–13

Roullet G, Madec G (2000) Salt conservation, free surface, and varying levels: a new formulation for ocean general circulation models. J Geophys Res 105(C10):23927–23942

Saji NH, Goswami BN, Vinayachandran PN, Yamagata T (1999) A dipole mode in the tropical Indian Ocean. Nature 401:360–363

Schwarzkopf FU, Böning CW (2011) Contribution of Pacific wind stress to multi-decadal variations in upper ocean heat content and sea level in the tropical south Indian Ocean. Geophys Res Lett 38:L12602. doi:10.1029/2011GL047651

Sengupta D, Senan R, Goswami BN, Vialard J (2007) Intraseasonal variability of equatorial Indian Ocean zonal currents. J Clim 20:3036–3055

Shankar D, Shetye SR (1999) Are interdecadal sea level changes along the Indian coast influenced by variability of monsoon rainfall? J Geophys Res 104:26031–26042

Sverdrup HU (1947) Wind driven currents in a baroclinic ocean, with application to the equatorial currents of the eastern Pacific. Proc Natl Acad Sci USA 33:318–326

Taylor KE, Stouffer RJ, Meehl GA (2012) An overview of CMIP5 and the experiment design. Bull Am Meteor Soc. 93. doi: 10.1175/BAMS-D-11-00094.1

Timmermann A, McGregor S, Jin FF (2010) Wind effects on past and future regional sea level trends in the southern Indo-Pacific. J Climate 23:4429–4437

Tokinaga H, Xie SP (2011) Wave and anemometer-based sea surface wind (WASWind) for climate change analysis. J Climate 24:267–285

Tokinaga H, Xie SP, Timmermann A, McGregor S, Ogata T, Kubota H, Okumura YM (2012) Regional patterns of tropical Indo-Pacific climate change: evidence of the walker circulation weakening. J Climate 25:1689–1710

Tozuka T, Yokoi T, Yamagata T (2010) A modeling study of interannual variations of the Seychelles dome. J Geophys Res 115:C04005

Ummenhofer CC, England MH, McIntosh PC, Meyers GA, Pook MJ, Risbey JS, Gupta AS, Taschetto AS (2009) What causes southeast Australia's worst droughts? Geophys Res Lett 36:L04706. doi:10.1029/2008GL036801

Unnikrishnan AS, Shankar D (2007) Are sea level-rise trends along the coasts of north Indian Ocean coasts consistent with global estimates? Global Planet Change 57:301–307

Uppala SM et al (2005) The ERA-40 re-analysis. Q J R Meteorol Soc 131:2961–3012

Vecchi GA, Soden BJ (2007) Global warming and the weakening of the tropical circulation. J Climate 20:4316–4340

Vecchi GA, Soden BJ, Wittenberg AT, Held IM, Leetmaa A, Harrison MJ (2006) Weakening of tropical Pacific atmospheric circulation due to anthropogenic forcing. Nature 441:73–76

Vialard J, Menkes C, Boulanger JP, Delecluse P, Guilyardi E, McPhaden M (2001) A model study of the oceanic mechanisms affecting the equatorial SST during the 1997–98 El Niño. J Phys Oceanogr 31:1649–1675

Vialard J, Shenoi SSC, McCreary JP, Shankar D, Durand F, Fernando V, Shetye SR (2009) Intraseasonal response of northern Indian Ocean coastal waveguide to the Madden-Julian Oscillation. Geophys Res Lett 36:L14606

Vimont DJ (2005) The contribution of the interannual ENSO cycle to the spatial structure of decadal ENSO-like variability. J Climate 18:2080–2092

Webster PJ, Moore AM, Loschnigg JP, Leben RR (1999) Coupled oceanic-atmospheric dynamics in the Indian Ocean during 1997–98. Nature 401:356–360

Wijffels S, Meyers G (2004) An intersection of oceanic wave guides: variability in the Indonesian throughflow region. J Phys Oceanogr 34:1232–1253

Wirth A, Willebrand J, Schott F (2002) Variability of the Great Whirl from observations and models. Deep-Sea Res II 49:1279–1295

Woodruff SD, Worley SJ, Lubker SJ, Ji Z, Freeman JE, Berry DI, Brohan P, Kent EC, Reynolds RW, Smith SR, Wilkinson C (2011) ICOADS release 2.5: extensions and enhancements to the surface marine meteorological archive. Int J Climatol 31: 951–967

Woodworth PL, Player R (2003) The permanent service for mean sea level: an update to the 21st century. J Coastal Res 19:287–295

Yin X, Gleason BE, Compo GP, Matsui N and Vose RS (2008) The International Surface Pressure Databank (ISPD) land component version 2.2. National Climatic Data Center: Asheville NC. Available from ftp://ftp.ncdc.noaa.gov/pub/data/ispd/doc/ISPD 22.pdf

Yu B, Zwiers FW (2010) Changes in equatorial atmospheric zonal circulations in recent decades. Geophys Res Lett 37:L05701

Yu W, Xiang B, Liu L, Liu N (2005) Understanding the origins of interannual thermocline variations in the tropical Indian Ocean. Geophys Res Lett 32:L24706

Zhang C (2005) Madden-Julian Oscillation. Rev Geophys 43:RG2003

Zhang X, Church JA (2011) Linear trend of regional sea level change in the Pacific Ocean and its relationship with background decadal oscillation. Submitted to J Climate

Zhang D, McPhaden MJ (2006) Decadal variability of the shallow Pacific meridional overturning circulation: relation to tropical sea surface temperatures in observations and climate change models. Ocean Modell 15:250–273

Zhang Y, Rossow WB, Lacis AA, Oinas V, Mishchenko MI (2004) Calculation of radiative fluxes from the surface to top of atmosphere based on ISCCP and other global data sets: refinements of the radiative transfer model and the input data. J Geophys Res 109:1–27

Zhang X, Lu Y, Thompson KR (2009) Sea level variations in the tropical pacific ocean and the Madden–Julian Oscillation. J Phys Oceanogr 39:1984–1992